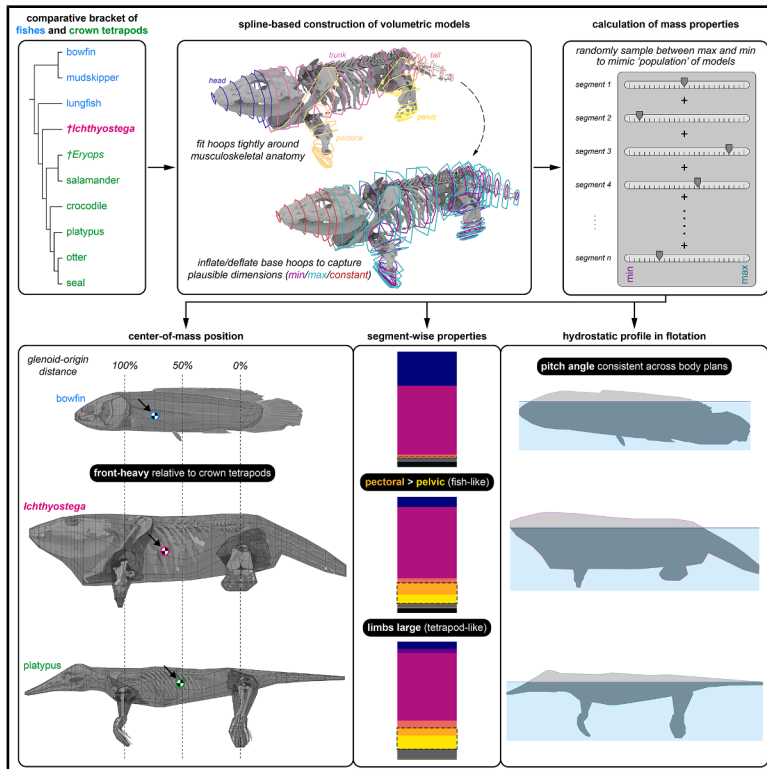


Digital volumetric modeling reveals unique body plan experimentation in the Devonian tetrapod *Ichthyostega*

Graphical abstract



Authors

Catherine R.C. Strong, Peter J. Bishop, John R. Hutchinson, Stephanie E. Pierce

Correspondence

crstrong@g.harvard.edu (C.R.C.S.), spierce@oeb.harvard.edu (S.E.P.)

In brief

Evolutionary biology; Biomechanics; Paleobiology

Highlights

- Fishes and tetrapods exhibit “front-heavy” versus “limb-centric” body plans
- *Ichthyostega* shows a unique mixture of fish- and tetrapod-like body proportions
- Mass properties of *Ichthyostega* support forelimb-dominated movement on substrate
- Body plan does not impact hydrostatic profile at flotation equilibrium



Article

Digital volumetric modeling reveals unique body plan experimentation in the Devonian tetrapod *Ichthyostega*

Catherine R.C. Strong,^{1,4,5,*} Peter J. Bishop,^{1,2,4} John R. Hutchinson,³ and Stephanie E. Pierce^{1,*}¹Museum of Comparative Zoology and Department of Organismic and Evolutionary Biology, Harvard University, Cambridge, MA 02138, USA²Geosciences Program, Queensland Museum, Brisbane, QLD 4011, Australia³Structure and Motion Laboratory, Royal Veterinary College, Hatfield, Hertfordshire AL97TA, UK⁴These authors contributed equally⁵Lead contact*Correspondence: crstrong@g.harvard.edu (C.R.C.S.), spierce@oeb.harvard.edu (S.E.P.)<https://doi.org/10.1016/j.isci.2025.112486>

SUMMARY

The water-to-land transition in tetrapods promoted a radical shift in locomotor function and kinematic patterns, from axial- to appendicular-dominated propulsion and from buoyancy- to musculoskeletal-driven support. Many of these facets of locomotion are dictated by an animal's whole-body mass properties, which presumably also changed across this transition. We herein use digital volumetric modeling to reconstruct mass properties in the Late Devonian tetrapod *Ichthyostega*. In comparison to fishes and crown tetrapods, our results show that *Ichthyostega* possessed a uniquely “robust” body plan, combining traits typical of both “fishes” (anterior center-of-mass) and “tetrapods” (well-developed limbs, especially forelimbs). We also find that variation in body composition has little effect on body attitude at flotation equilibrium, suggesting that whole-body “evolutionary tinkering” had little impact on hydrostatic profile. These results support previous inferences of forelimb-dominated movements in *Ichthyostega* and highlight a hitherto underappreciated level of morphological experimentation during the tetrapod transition to land.

INTRODUCTION

The water-to-land transition in tetrapods was one of the most transformational events in the history of animal life. Escaping the water enabled adaptive radiations of diverse lineages that came to inhabit terrestrial, aerial, and (ironically) aquatic environments, shaping the course of life over 300+ million years.¹ Over the past four decades, burgeoning fossil discoveries have dramatically refined, and indeed redefined, our understanding of many aspects of this event (see review by Ahlberg²). At the broadest level, the transition from fish to tetrapod—here taken to mean vertebrates with digit-bearing limbs as opposed to fins—is now recognized as having temporally preceded the transition from water to land, possibly by tens of millions of years.^{1,3–6} Both transitions involved radical changes to every component of the vertebrate bauplan, including reconfiguration of the skull, braincase and jaws,^{1,7–10} reflecting changes to feeding,^{11,12} breathing,^{5,13} and sensation^{14,15}; development of a mobile neck¹⁶; increased complexity of the vertebral column and ribs^{4,17–19}; consolidation of the appendicular skeletal structure and articulations,^{20–23} including the appearance of digits^{3,24,25}; and increased development and differentiation of appendicular musculature.^{26–29}

A central factor shaping these myriad anatomical, functional, and physiological transformations was the stark contrast in

physical properties between aquatic and terrestrial environments. In the context of locomotion, order-of-magnitude differences in the density and viscosity of water versus air greatly influence the efficacy of different strategies in generating thrust (propulsion and braking) and supporting the body against gravity.^{30,31} With the transition to terrestrial (subaerial) environments, reliance on the buoyancy of high-density water for external gravitational support had to be replaced by an internal source of support via sufficiently strong axial and appendicular musculoskeletal systems. The vastly lower density of air also meant that fluid-acceleration mechanisms of thrust generation (i.e., via fin-based lift) were ineffective. Simultaneously, the lower viscosity of air reduced unwanted drag, effectively eliminating selective pressures for anatomical streamlining. These differences collectively necessitated the evolution of—and reliance upon—substrate-associated terrestrial locomotion, including a shift from axial-to appendicular-dominated propulsion mechanisms. As part of navigating this ecological interface, novel locomotor modes would have helped to offset the increased effects of gravity as vertebrates first ventured onto land.^{32–34} Ultimately, these physical constraints led to the development and elaboration of new patterns of coordination between the appendicular and axial systems, such as the lateral sequence gait characteristic of most extant tetrapods,^{35,36} with the vertebral column oscillating in standing waves.^{37,38}



Deciphering the timing and sequence by which terrestrial tetrapod locomotion evolved has proven a considerable challenge. Although tetrapods have traditionally been characterized as employing a lateral sequence gait, in which the limbs move in a coordinated and alternating manner and the hindlimbs drive propulsion against the substrate,^{2,37,39–42} recent studies have complicated this perspective: Some authors have contended a more widespread distribution of these features among non-tetrapod vertebrates (see e.g.,^{41,43}), whereas others have conversely posited a more restricted distribution among only a subset of tetrapods (see e.g.,^{33,34,44}). This uncertainty is due in no small part to the incompleteness of the fossil record, combined with the often confusing juxtaposition of (seemingly) aquatic or terrestrially adapted features in various taxa.^{1,5,22,33} Drawing qualitative analogies with potential extant analogs for tetrapodomorph fishes or early evolving tetrapods can provide perspective, but this approach is often limited by the sheer morphological and phylogenetic disparity separating extant taxa from the extinct species-of-interest.⁴⁴ An alternative strategy is to integrate fossil data with extant anatomy in a framework grounded in physical principles that apply universally to all species (e.g., Bishop et al.⁴⁵). Such biomechanically informed analyses can provide a quantitative means to evaluate functional hypotheses regarding the fish–tetrapod transition,^{11,33,34,46,47} especially when strongly contrasting physical contexts are involved.

Despite the stark differences between aquatic and terrestrial settings, one facet crucial to locomotion in both environments is an animal’s mass properties. Body mass must be supported against gravity in both environments, but increases with linear dimensions (i.e., “size”) more rapidly than the ability of bone and muscle tissues to support it.^{31,48} Although supported by buoyancy in aquatic settings, body mass must still be appropriately tuned to body dimensions to achieve an appropriate bulk density for navigating the water column. The spatial distribution of mass throughout the body is also important, as this configuration determines the position of the net gravity vector, which acts through the center of mass (COM). On land, the position of the COM with respect to the pectoral and pelvic girdles determines differential body weight support and thrust generation by the fore- and hindlimbs.^{43,49–51} In the water, COM location influences the attitude and stability of the body when immersed.^{52,53} Quantifying mass and its distribution in stem tetrapods (both finned and limbed) can therefore provide insight into major functional transformations at the interface of water and land. For example, an anteriorly displaced COM would imply a greater role of the forelimbs in body support and movement (e.g.,^{33,49–51}), while investigating the impact of COM on buoyancy-related properties can reveal how reconfigurations to the body plan would have affected hydrostatic profile.

As one of the oldest known (Late Devonian, ~360–365 Ma) tetrapods documented by abundant fossil material, the iconic *Ichthyostega* has historically served as the archetypal intermediate between “fish” and “tetrapod”.^{7,54} This taxon has therefore played a major role in interpreting the pattern of anatomical, functional, and physiological transformation between fish and tetrapod body plans.^{1,3,7,54–56} Yet, numerous studies have highlighted the at-times surprising cranial and postcranial anatomy of

this animal, indicating notable ecological divergence even among Devonian tetrapods and questioning assumptions about the paleobiology of these animals.^{2,8,14,17,18,22,33,47,57} Insofar as locomotion is concerned, substantial vertebral regionalization and restricted fore- and hindlimb joint mobility together suggest use of an atypical locomotor mode, akin to the terrestrial “crutching” behavior of mudskippers.^{17,18,33} Indeed, the articular geometry of the joints outright precludes the use of limb postures typical of commonly invoked extant tetrapod analogs (e.g., salamanders), instead demonstrating that the hindlimbs were unable to make notable traction with the substrate; this posture would have rendered the hindlimbs essentially ineffective on land, but potentially quite useful as paddles underwater.³³ Further complicating assessments, *Ichthyostega* possesses well-ossified ribs and robust limb girdles suggestive of terrestrial competence,⁵⁸ alongside aquatic traits including a fish-like tail, lateral line canals, deeply grooved gill bars, and an ear apparently specialized for underwater hearing.^{14,59} Thus far, quantitative assessments of this enigmatic animal have yet to take a whole-animal perspective, although, as one of the few Devonian tetrapods known from essentially the entire skeleton, such approaches are ripe for the undertaking.

In this study, we draw upon a previous three-dimensional (3D) whole-skeleton reconstruction³³ to explore the body plan of *Ichthyostega*, providing the first detailed, quantitative assessment of mass properties in any stem tetrapod. Building upon an extensive literature of digital volumetric modeling in extant and extinct species,^{52,53,60–64} we expand upon prior approaches in both phylogenetic scope and methodological sophistication. We extend investigation to the pre-Permian fossil record for the first time (Figure 1A) and develop strategies for simulating population-level variation in body morphology, permitting a more in-depth assessment of intraspecific variation in whole-body and segment-wise properties (Figures 1B and 1C). We also perform simulations of flotation equilibrium to glean insight into aquatic locomotor proficiency (Figure 1D). Contextualizing the mass properties of *Ichthyostega* in relation to an ecomorphologically diverse sample of fishes and crown tetrapods (Figure 1A), we provide new insight into body plan construction, locomotor modes, and aquatic proficiency in this key stem tetrapod. Overall, our analyses enable a more comprehensive and nuanced assessment of anatomical specialization, morphological diversification, and locomotor function across the fish–tetrapod transition.

RESULTS

Using 3D skeletal geometries as a guide (Data S1), we digitally reconstructed soft-tissue geometries—representing both flesh volumes and air cavities (e.g., lungs)—for *Ichthyostega*,³³ three extant fishes, one extinct crown tetrapod, and five extant crown tetrapods (Figure 1A; Table S1; Data S2 and S3). Prior reconstructions^{7,17,54} have portrayed *Ichthyostega* with similarly sized fore- and hindlimbs, in contrast to the proportionally larger pectoral skeleton of our model³³; therefore, to assess the effect of these differing reconstructions, we also created two additional variants of the base *Ichthyostega* model, with the hindlimb volumes “scaled up” (Figure S1). We constructed all models using

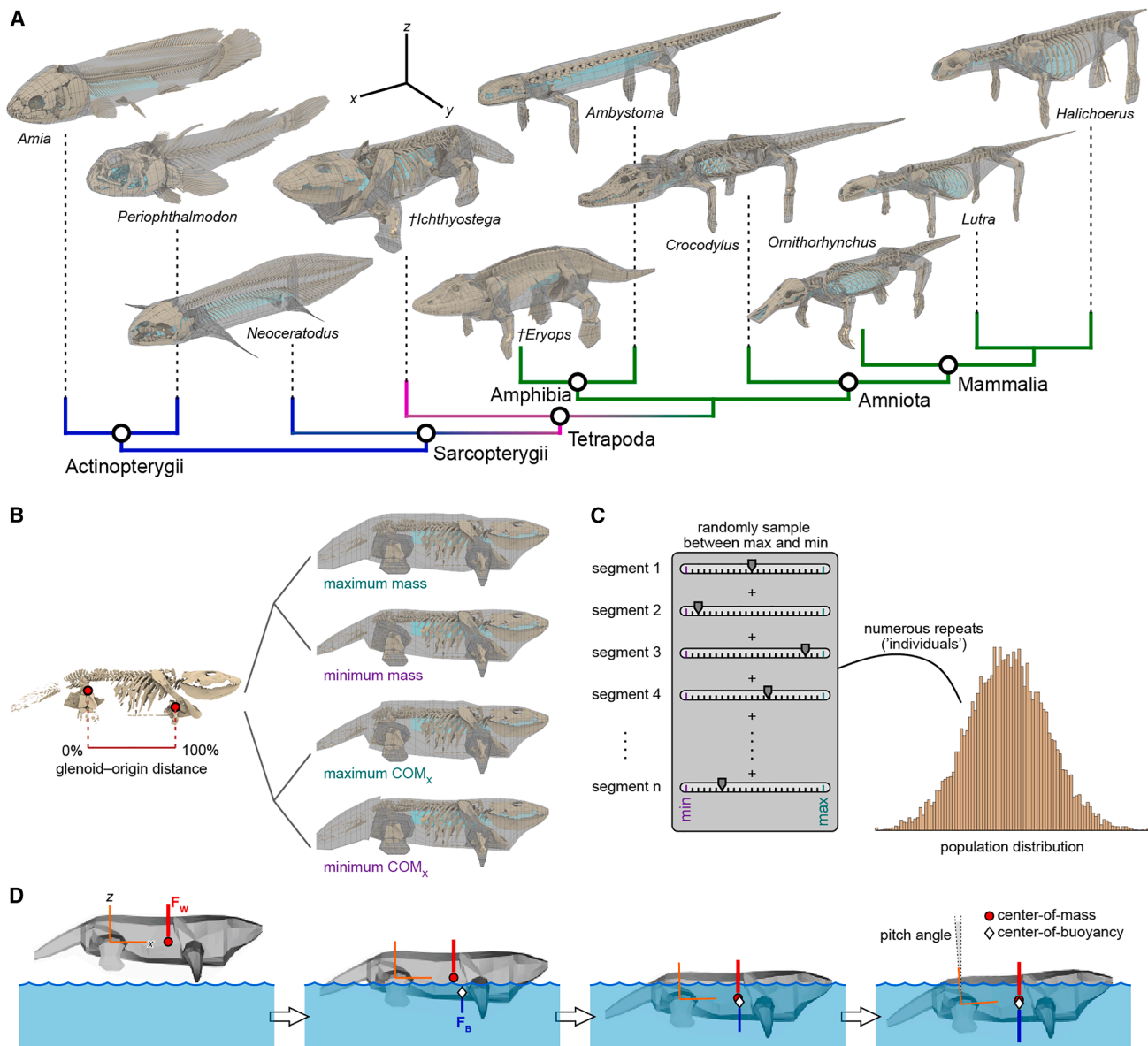


Figure 1. Reconstructing mass properties in *Ichthyostega* alongside a phylogenetic and ecofunctional bracket of potential extant analogs

(A) Taxon sample, showing phylogenetic relationships and “minimal mass” flesh reconstructions (in oblique lateral view, not to scale). Gray denotes flesh, turquoise denotes zero-density air spaces. See also Figures S2 and S3; Data S1–S2.

(B) Reconstructing upper and lower bounds on body mass and anteroposterior center-of-mass (COM_x) position. See also Data S2–S3 and Code S3.

(C) Using Monte Carlo resampling of each segment’s mass properties to emulate population-level variation in whole-animal mass properties. See also Data S2, Data S4, and Code S1.

(D) Determining flotation equilibrium via pseudo-dynamic simulation; equilibrium is reached when the downward force due to body weight (F_w) and the upward force due to buoyancy (F_b) are equal in magnitude and collinear. The resulting attitude of the body (e.g., sagittal pitch angle) can then be measured. See also Data S3–S4 and Code S2.

a hoop-based “spline” method,^{61,62,65} guided by the underlying skeletal and inferred muscular anatomy (Figures S2 and S3); this approach enabled the creation of plausible “maximum” and “minimum” volumes for each body segment (Data S2)—and, in turn, the overall body (Figure 1B; Data S3)—thus facilitating assessment of intra- and interspecific variation in mass properties (Figure 1C; Tables S2–S4; Data S4) and their possible effects

on terrestrial and aquatic locomotion (Figure 1D). Full details are provided in the STAR Methods (see also Code S1–S4).

Mass estimates

Our “best-estimate” model of *Ichthyostega* yields a whole-body mass of 3.66–5.08 kg, with a mean of 4.40 kg (Figure 2; Table S2; Data S4). Increasing the hindlimb volume of *Ichthyostega* results

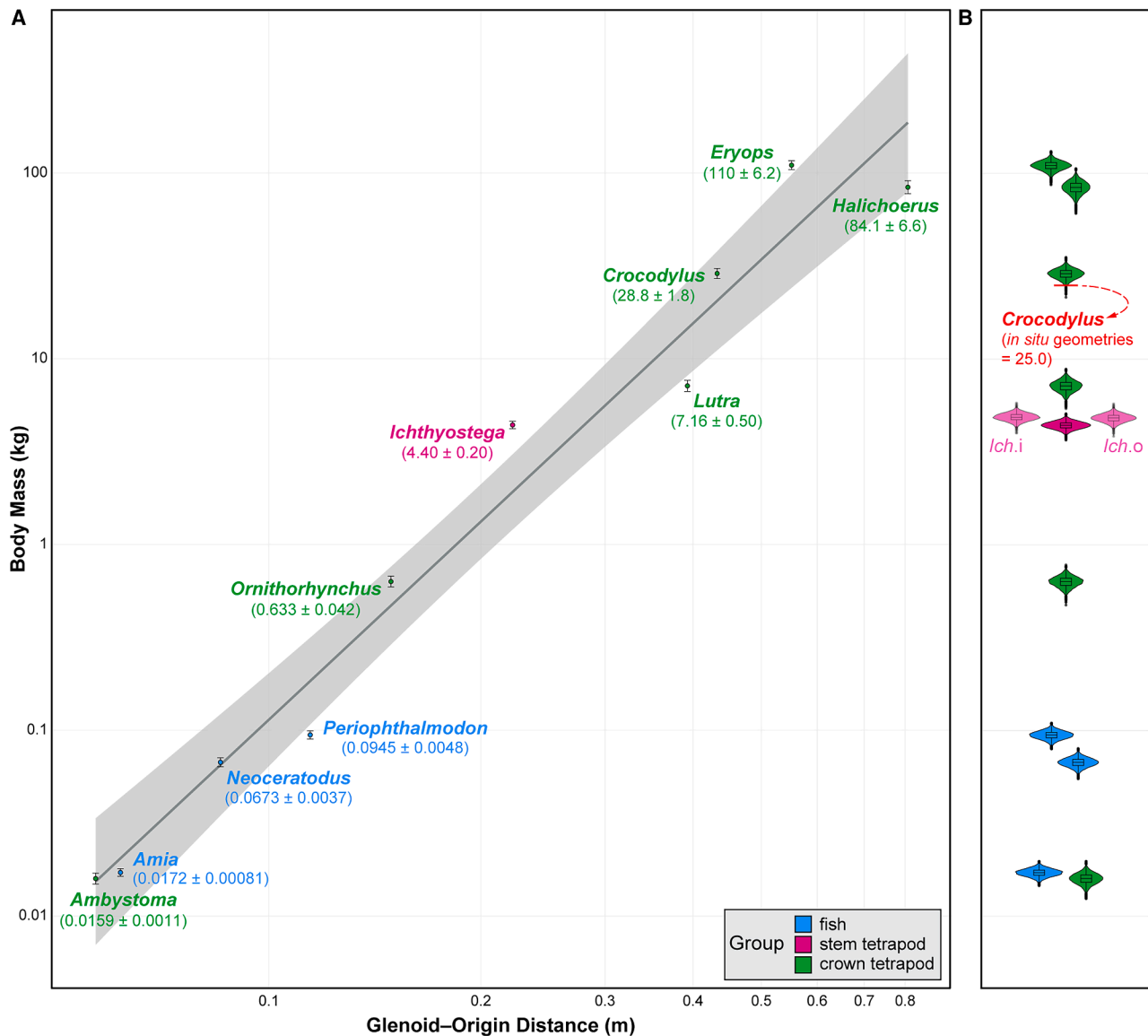


Figure 2. Whole-body mass estimates, obtained by combining mass properties drawn randomly from a normal distribution for each segment ($n = 10,000$ replicates per taxon, flesh density = 1000 kg/m^3)

(A) Scaling of mean body mass against glenoid–origin distance. Error bars indicate \pm one standard deviation; mean body mass (in kg) and standard deviation indicated in parentheses for each taxon. Gray line represents an ordinary least-squares regression and 95% confidence interval. Data are \log_{10} -transformed; axes re-labeled with corresponding non-logged values for clarity.

(B) Distribution of estimated body mass values for each taxon. Violin plots depict the overall density of the data, with inlaid boxplots denoting the interquartile range and outlying values. Red line indicates the mass of *Crocodylus* as determined using meshes of the actual flesh and air volumes. Additional hindlimb variants for *Ichthyostega* (“inflated” and “overall”; see STAR Methods) are rendered transparent. See also Data S2, Data S4, Code S1, and Code S4.

in slightly higher estimates of body mass (*Ichthyostega*.inflated: mean = 4.88 kg, range = 4.00–5.80 kg; *Ichthyostega*.overall: mean = 4.82 kg, range = 3.84–5.74 kg), although these values nonetheless remain largely within the range recovered for our “best-estimate” model (Figure 2B). Contextualized against a range of ecofunctional analogs, *Ichthyostega* evinces a more “robust” overall body plan given the scaling relationship across the overall dataset, with a comparatively high body mass relative to its body length (Figure 2A). This robustness also appears in the

extinct *Eryops*, with our model of this latter taxon yielding an estimated mass of 86.88–131.42 kg (mean = 110.28 kg). These results for *Eryops* are consistent with mass estimates derived from minimum convex hull–based methods applied to the same specimen in previous work (104 kg⁷⁹).

Center-of-mass estimates

For each model variant created in our workflow, we computed the whole-body COM position as a percentage of glenoid–origin

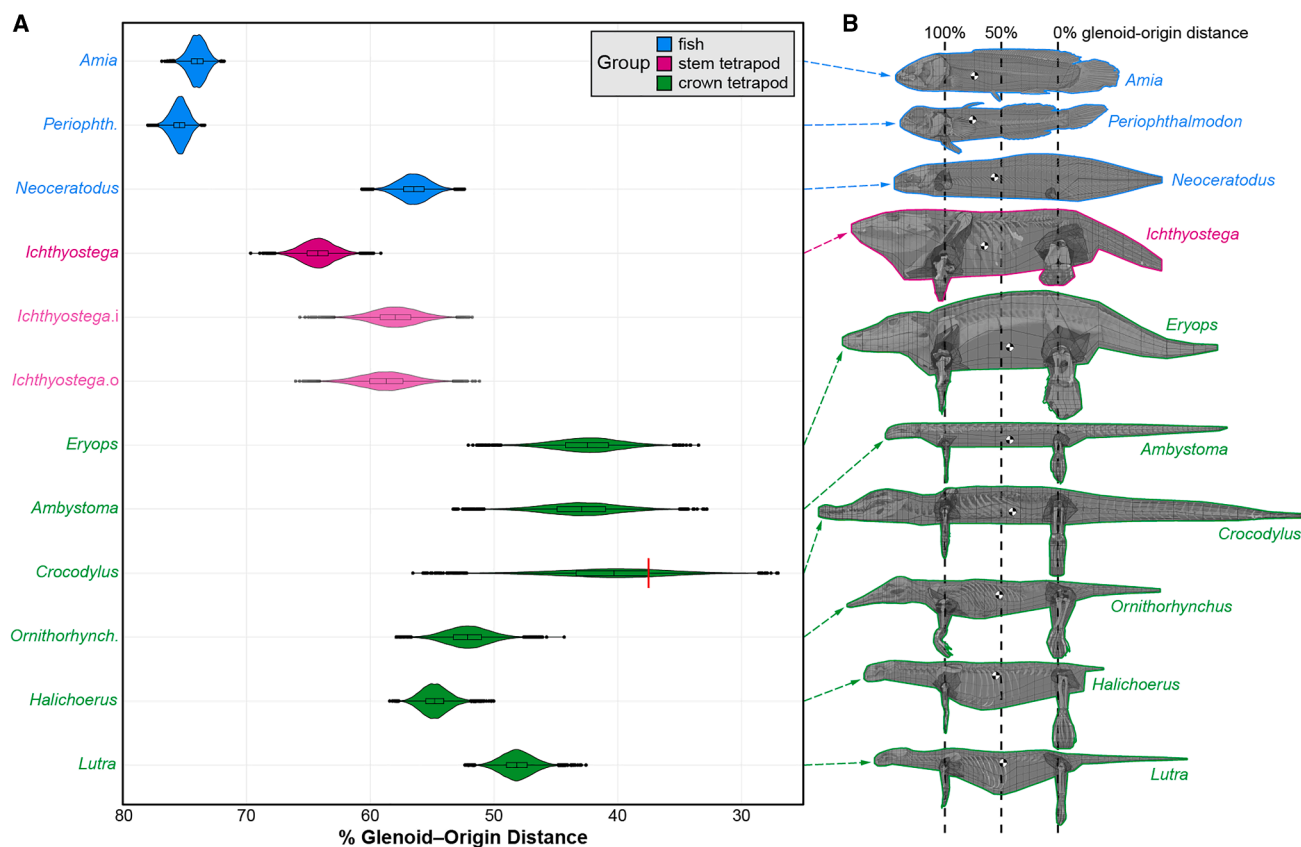


Figure 3. Whole-body anteroposterior center-of-mass (COM_x) position, obtained by combining mass properties drawn randomly from a normal distribution for each segment ($n = 10,000$ replicates per taxon, flesh density = 1000 kg/m^3)

(A) Distribution of estimated COM_x position for each taxon, normalized as a percentage of glenoid–origin distance. Higher values indicate a more anteriorly positioned COM. Violin plots depict the overall density of the data, with inlaid boxplots denoting the interquartile range and outlying values. Red line indicates the COM_x of *Crocodylus* as determined using meshes of the actual flesh and air volumes. Additional hindlimb variants for *Ichthyostega* (“inflated” and “overall”; see STAR Methods) are rendered transparent.

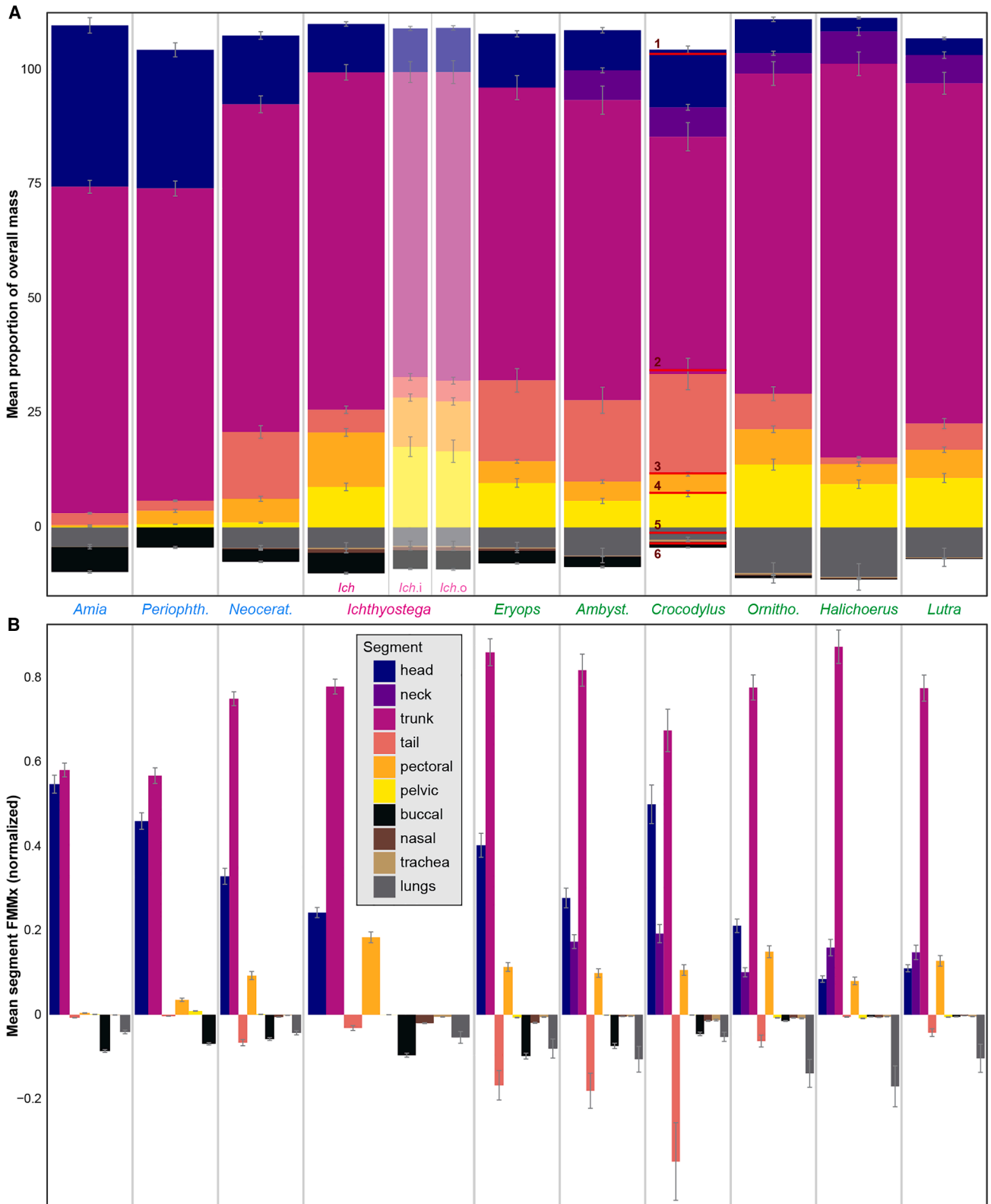
(B) Graphical depiction of mean COM_x position, using “minimal mass” flesh reconstructions in lateral view. Images scaled to equal glenoid–origin distance for visualization. See also Data S2, Data S4, Code S1, and Code S4.

distance (GOD) (Figure 3; Table S2; Data S4), with the origin set at the pelvis for tetrapods and at the caudal fin base for fishes (see STAR Methods for further explanation). Our analysis recovers a clear separation in anteroposterior COM position (COM_x) for actinopterygians versus sarcopterygians (including tetrapods), with the former exhibiting a more anteriorly positioned COM (Figure 3). Among the sarcopterygians in our sample, *Ichthyostega* has the most anteriorly positioned COM, with a mean COM_x of 64.3% GOD. Indeed, its range of estimated COM_x positions (59.1–69.7% GOD) overlaps only with the Australian lungfish (*Neoceratodus*: mean = 56.5% GOD, range = 52.4–60.7% GOD); among the tetrapods modeled here, only the platypus (*Ornithorhynchus*: mean = 52.1% GOD, range = 44.3–57.9% GOD) and gray seal (*Halichoerus*: mean = 54.8% GOD, range = 50.0–58.4% GOD) exhibit a mean COM_x of >50% GOD, with even these values failing to overlap the COM_x position of *Ichthyostega*. As expected, increasing the hindlimb volume of *Ichthyostega* draws the COM_x more posteriorly (*Ichthyostega.inflated*: mean = 58.0% GOD, range = 51.8–65.7% GOD; *Ichthyostega.overall*: mean = 58.7% GOD, range = 51.2–66.0% GOD);

however, even in these model variants, *Ichthyostega* retains the anteriormost COM_x position among sarcopterygians, and especially tetrapods.

Segment-wise contributions to mass and COM

To understand the proximate cause of the distinctive COM_x position of *Ichthyostega* among our taxon sample, we assessed the individual contribution of each body segment to whole-body mass and COM (Figure 4; Table S3; Data S4). This segment-wise analysis reveals that the unique status of *Ichthyostega* is driven in large part by trends in the appendicular skeleton. In fishes, the pectoral segment is consistently more massive than the pelvic segment, but together these comprise only a small proportion of overall body mass (Figure 4A); in turn, whole-body COM_x is determined predominantly by the head and trunk (Figure 4B). In contrast, crown tetrapods possess proportionally much larger appendicular segments, with the pelvic segment now being consistently more massive than the pectoral segment (Figure 4A). However, despite a much greater pectoral contribution in “pulling” the overall COM_x position anteriorly, this effect is



(legend on next page)

outweighed by notable negative contributions from the tail and lungs (Figure 4B), such that the whole-body COM_x of crown tetrapods is ultimately posterior to that of fishes, especially actinopterygians (Figure 3; Table S2). Our results show that the body plan of our “best-estimate” *Ichthyostega* model stands in contrast to both of these patterns: unlike the fishes in our sample, the appendicular segments of *Ichthyostega* comprise a major component of its body mass; but, unlike the crown tetrapods, the mass of the pectoral segment exceeds that of the pelvic segment (Figure 4A). *Ichthyostega* is further distinctive in exhibiting the highest pectoral first mass moment (FMM_x), meaning that its pectoral segment contributes more to whole-body COM_x than in any other taxon sampled (Figure 4B).

Unsurprisingly, increasing the hindlimb volume of *Ichthyostega* results in a body plan more akin to other tetrapods, in that the relative mass of the pelvic segment in the “inflated” and “overall” *Ichthyostega* models ultimately exceeds that of the pectoral segment (Figure 4A). Indeed, because the pectoral girdle and limbs are much larger relative to the body than in other tetrapods, these hindlimb variants ultimately result in the highest contribution of the pelvic segment to overall body mass across our sample (Figure 4A). Note that this does not affect segment-wise FMM_x compared to our “best-estimate” model of *Ichthyostega* (Table S3): because our global coordinate system is centered between the acetabula for tetrapods, the FMM_x of the pelvic segment is inherently close to zero across our sample, regardless of pelvic mass. Overall, even if these alternative hindlimb reconstructions were to be preferred over the original composite,³³ the resultant body compositions would still be unique among the tetrapods sampled herein, with the largest hindlimbs relative to overall body mass and by far the greatest contribution of the limbs to overall body mass (28.4% and 27.5% of overall mass in *Ichthyostega.inflated* and *Ichthyostega.overall*, respectively, versus 21.4% in *Ornithorhynchus*, the tetrapod with the next greatest contribution to mass from the limbs) (Figure 4A; Table S3).

Flotational equilibrium

To explore how body proportions may influence aquatic proficiency across our taxa, we performed simulations of flotational equilibrium in the sagittal plane (Figure 1D; Data S3), following the general approach of prior studies by Henderson.^{52,53} Our analysis tackled this topic from an explicitly comparative perspective, investigating how each of our models would be positioned given the same scenario (i.e., were the animal to come to equilibrium at the water’s surface), and how differences in body plan might affect this positioning (i.e., controlling for confounding effects such as tissue density). In other words, given

the same baseline scenario, how does body shape influence hydrostatic profile?

Equilibrium occurs when the downward force of body weight is balanced by the upward force of buoyancy, and the model’s COM is vertically aligned with its center-of-buoyancy (COB). In all taxa, equilibrium was reached with the COB positioned below the COM (Figure 5C; Table S4). This condition technically constitutes an “unstable equilibrium”,⁵³ requiring active generation of thrust from the tail, body, or fins/limbs to avoid rolling onto the side in the face of external perturbations; however, as the vertical distance between the COB and COM is always quite small (Figure 5C; Table S4), such restorative thrust would not need to be very large. As the horizontal distance between these values tends toward zero at equilibrium, trends in anteroposterior COB position (COB_x) match those recovered for COM_x (Figures 3A and 5A; see “center-of-mass estimates” above).

Notably, despite the marked variation in body shape and COM position across the taxa sampled herein, all attain a similar whole-body attitude at flotational equilibrium, with a modest nose-up pitch (Figure 5B; Table S4). Overall pitch, and variation therein, tends to be lower in crown tetrapods compared to fishes, but the magnitude of difference across our sample is small and likely not biologically meaningful; changes in body positioning could easily produce larger changes to pitch.^{52,66} Indeed, repositioning of the *Eryops* model to have the head and axial skeleton fully straightened out changed the pitch by up to 9.5° (Table S4).

Model evaluation

To test our overall approach to body mass modeling, we also performed all analyses using *in situ* flesh and air-space geometries of our *Crocodylus* specimen. The mass properties obtained using these known volumes are consistent with those obtained for our crocodile model across all analyses: the known flesh and air volumes yield a whole-body mass of 24.96 kg and a COM_x of 37.5% glenoid–origin distance, both of which fall within the respective ranges estimated for our crocodile model (mass: mean = 28.8 kg, range = 21.53–35.35 kg; COM_x : mean = 40.5% GOD, range = 27.0–56.6% GOD) (Figures 2 and 3; Table S2); and, the actual body mass of the original *Crocodylus* specimen was 27.7 kg, falling within the range of our results. Additionally, the segment-wise masses and FMM_x of the known versus modeled crocodile geometries compare quite closely (Figure 4; Table S3), and the COB_x (38.0% GOD) and pitch angle (5.6°) of the known crocodile geometries both fall within the respective ranges estimated for the crocodile model (COB_x : mean = 42.1% GOD, range = 21.3–59.8% GOD; pitch angle: mean = 4.8°, range = 3.2–7.8°) (Figure 5; Table S4).

For our fish models, we placed the global origin at the base of the caudal fin, a position which we deemed functionally

Figure 4. Mean segment-wise mass properties, obtained by averaging mass properties drawn randomly from a normal distribution for each segment ($n = 10,000$ replicates per taxon, flesh density = 1000 kg/m³)

(A) Mean contribution of each segment to overall body mass. Additional hindlimb variants for *Ichthyostega* (“inflated” and “overall”; see STAR Methods) are rendered transparent. Red lines indicate the segment-wise mass of *Crocodylus* as determined using meshes of the actual flesh and air volumes; 1, combined head + trunk; 2, tail; 3, pectoral; 4, pelvic; 5, buccal cavity; 6, combined nasal cavity + trachea + lungs.

(B) Mean anteroposterior first mass moment (FMM_x) of each segment, normalized by the product of whole-body COM_x and whole-body mass. See also Data S2, Data S4, Code S1, and Code S4.

Error bars indicate \pm one standard deviation.

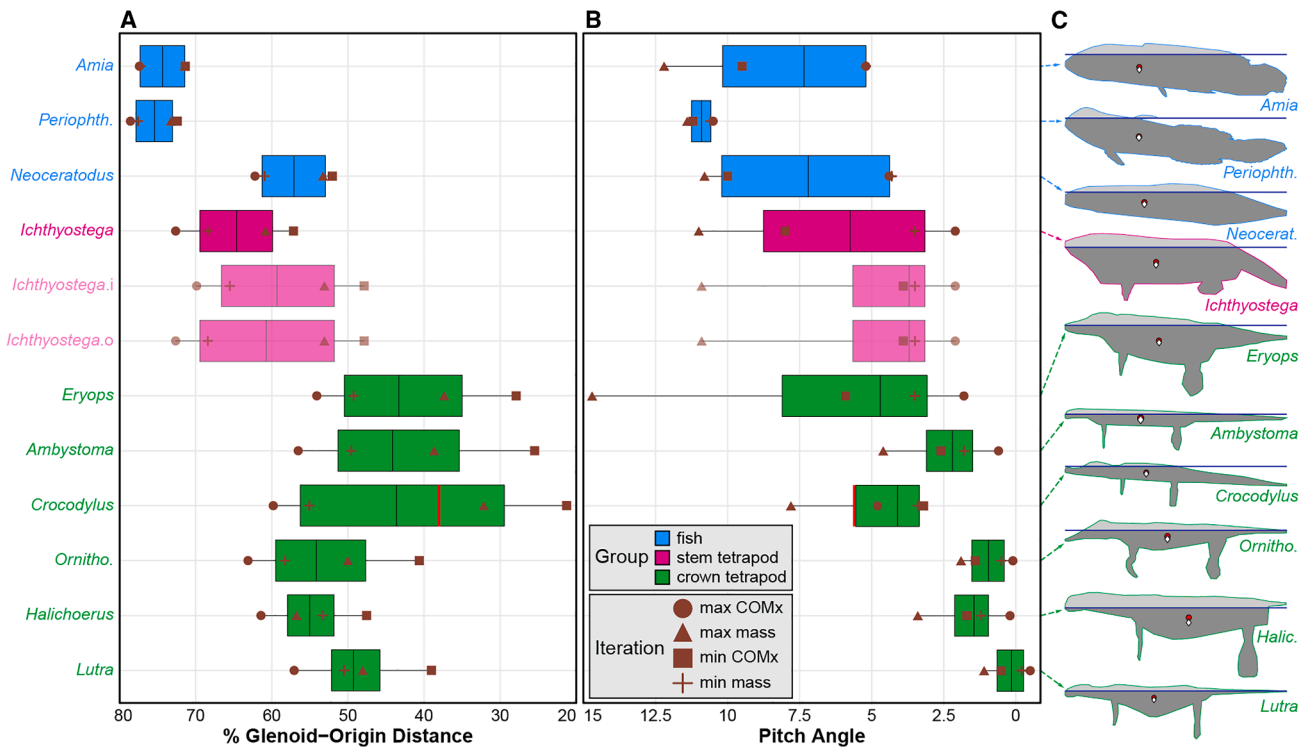


Figure 5. Buoyancy properties at flotational equilibrium across four “extremes” of body plan construction (flesh density = 1000 kg/m³)
 Red lines indicate the properties of *Crocodylus* as determined using meshes of the *in-situ* flesh and air volumes. Additional hindlimb variants for *Ichthyostega* (“inflated” and “.overall”; see STAR Methods) are rendered transparent.
 (A) Anteroposterior center-of-buoyancy (COB_x) for each taxon, normalized as a percentage of glenoid–origin distance. Higher values indicate a more anteriorly positioned COB.
 (B) Pitch angle about the origin at equilibrium; 0 represents a level (horizontal) pose with respect to the model reference position, with higher values indicating a greater nose-up pitch.
 (C) Silhouettes of “minimum mass” models at flotational equilibrium. Blue line, water-line; white diamond, center-of-buoyancy; red circle, center-of-mass. Images not to scale. See also Data S3–4 and Code S2–4.

consistent with the inter-acetabular global origin used for the tetrapod models (see STAR Methods for further explanation). Since the raw COM_x coordinates for each model iteration were normalized using glenoid–origin distance, we therefore tested how this choice of global–origin position in the fish models could affect our overall conclusions regarding COM_x trends. To do so, we re-normalized the raw COM_x coordinates for the fishes using three other potential global–origin landmarks: the posterior margin of the anal fin, the anterior margin of the anal fin, and the pelvis (Figure S4; Table S5). This comparison justifies our choice not to use the pelvis as the fish global–origin, seeing as this landmark simply emphasizes the extensively modified position of the pelvic fin in *Periophthalmodon* relative to the other taxa in our sample (Figure S4D). Regarding the anal fin, our overarching conclusions are robust regardless of which landmark is used in the fish models (Figure S4; Table S5). Specifically, placing the global origin at the posterior margin of the anal fin (Figure S4B) produces no notable differences compared to using the base of the caudal fin (as in our original analyses; see Figures 3 and S4A). Normalization using the anterior anal fin margin (Figure S4C) does result in a relatively more posterior COM_x position in actinopterygians, bringing these taxa more in

line with—although still generally more anterior to—the COM_x position recovered for crown tetrapods (overall mean = 56.45% [s.d. = 4.3] of glenoid–anterior anal fin distance in fishes versus 46.83% [s.d. = 5.9] of glenoid–acetabulum distance in crown tetrapods). Tied to this, the COM_x position of *Ichthyostega* would in turn now be slightly anterior to that of fishes (Figure S4C), rather than being intermediate between actinopterygians and sarcopterygians (including crown tetrapods) as in Figures S4A, S4B, and Figure 3. Nevertheless, the core result of “front-heavy fishes” versus “back-heavy crown tetrapods” still holds, and thus our overall conclusions as presented below regarding body plan innovation in *Ichthyostega* remain valid.
 The overall goal of our flotational simulations was to investigate how body plan impacts the whole-body orientation of each model, all else being equal (i.e., in the same scenario—at flotational equilibrium—and controlling for confounding effects such as tissue density). This approach is thus designed to reveal the effect of body shape alone on buoyancy-related properties, rather than to produce a “life-accurate” reconstruction of the habitual behaviors exhibited by any given animal (especially since animals can actively modulate whole-body density to achieve different subaqueous postures). Nonetheless, to

corroborate this analytical approach, it is still important to demonstrate that *in vivo* postures could indeed be recovered given the appropriate inputs. To test this outcome, we performed an additional set of flotational simulations designed to mimic “air-gulping” in *Amia* (Figure S5), given the availability of X-ray imagery of this behavior.⁶⁷ For these analyses, we divided the original “minimum-mass” air-cavity volume for *Amia* into three components reflecting the different phases of air-gulping (provided in Data S3), then performed simulations using each of these respective volumes (Figures S5A–S5C). The resultant buoyancy profiles are consistent with the various whole-body orientations observed *in vivo* throughout a cycle of air-gulping (i.e., as air passes through the buccal cavity to the lung) (Figures S5A–S5C), illustrating the ability of our simulations to accurately mimic a variety of subaquatic postures (see also Henderson⁵²). More broadly, the placement of the eyes, and often nostrils, above the water’s surface in most of our simulations (Figure 5) is consistent with behaviors typically observed *in vivo* in association with positive buoyancy, such as breathing and subaerial vision. Finally, although the orientation of the appendages during “actual” swimming may differ from the standardized reference pose used for our models, such differences would not affect hydrostatic profile at flotational equilibrium as long as the appendages are fully submerged; simplified models constructed to illustrate this principle achieved an identical disposition at flotational equilibrium (Figure S5D), with a nose-up pitch of 1.4°. Altogether, our simulations are therefore able both to recover “realistic” poses at flotational equilibrium and to reconstruct more nuanced postures or behaviors given the appropriate inputs.

DISCUSSION

The origin of tetrapods entailed one of the most dramatic transformations in vertebrate evolution.¹ Given its status as a key taxon documenting the transition from water to land,^{5,7,8,17,54} the Late Devonian tetrapod *Ichthyostega* has been included in numerous comparative studies of stem tetrapod paleobiology. However, the distinctive whole-body anatomy of this iconic animal has largely escaped detailed quantitative investigation,³³ with prior work typically being qualitative in nature (e.g.,^{3,8,14,17,18,22,28,29,54,57}), focusing on a restricted anatomical scale (e.g.,^{3,8,14,15,17,18,22,46,47,68,69}), and/or encompassing many taxa with *Ichthyostega* as a single data-point (e.g.,^{15,23,46,47,68–72}). We herein address this shortcoming by providing a targeted analysis of the body plan of *Ichthyostega*. Using digital volumetric modeling, we assessed the mass properties of *Ichthyostega* alongside a broad ecofunctional and phylogenetic bracket, spanning fishes to mammals. In comparison to most previous studies, which have focused their modeling efforts on crown tetrapods, our taxon sample reflects one of the most phylogenetically and morphologically disparate analyzed to date (Figure 1A). We also introduce a population-based approach to volumetric model generation, adding a further level of rigor (STAR Methods; Figures 1B and 1C): whereas previous studies have relied upon a small number of pre-set configurations delimiting plausible extrema in body form (if not a single “mean” model) to characterize a given taxon, our approach gen-

erates a hypothetical “population” of viable models, thus enabling a more comprehensive reconstruction of intra- and interspecific variation. Finally, we also present a user-friendly, interactive interface for conducting simulations of flotational equilibrium (STAR Methods; Figure 1D), which allows direct evaluation of a critical aspect of aquatic performance. Collectively, our thorough quantifications of the body plan of a key stem tetrapod taxon afford important insights into the evolution of form and function across the vertebrate water-to-land transition.

A longstanding point of contention regarding the origin of tetrapods concerns the acquisition of terrestrially adapted locomotion. Traditionally, features including hindlimb-dominated propulsion,^{2,40,42} a lateral sequence gait (i.e., a gait in which the limbs move in a coordinated and laterally alternating manner^{37,39}), and coupled retraction/rotation of the humerus and femur^{37,39} have been considered definitive hallmarks of tetrapod movement (see also Ahlberg²). However, certain extant taxa have been found to contravene this assumption. For example, when underwater, the African lungfish uses its pelvic fins to propel itself and hold the body off the substrate,⁴¹ with similar behaviors having also been observed in various skates.⁷³ Additionally, epaulette sharks employ coordinated pectoral and pelvic fin movements on submerged substrates, producing trotting gaits,⁴³ which differ from lateral sequence gaits only by a lack of phase offset between front and rear fin pairs. These observations suggest that some putatively “tetrapod-specific” features of locomotion are in fact more widespread among vertebrates that engage in substrate-based locomotion.

Further complicating matters, some of these presumed hallmarks of modern tetrapod locomotion have more recently been suggested as absent in some stem taxa from the Devonian Period,^{33,34,44} conversely implying a more restricted distribution of these features, arising sometime after the origin of tetrapods. This latter perspective was advocated by Pierce et al.,³³ whose analysis of limb joint mobility in *Ichthyostega* revealed an inability to emplace the hindfeet on the ground (thus precluding hindlimb propulsion on land) or to notably rotate the humerus and femur about their long axes (as occurs during a lateral sequence gait in sprawling tetrapods³⁷). Rejecting a capacity for “typical” tetrapod locomotion, these authors instead proposed that *Ichthyostega* would have employed a mudskipper-like, forelimb-crutching gait on land and a hindlimb-driven paddling in the water. Although we do not directly assess locomotor dynamics in the present study, our analyses of mass properties across various fish and tetrapod body plans nonetheless provide key bearing on this hypothesis.

COM position is particularly relevant in this regard, as this property is linked closely to differential weight support by the appendicular skeleton on land^{43,49,50} and body attitude and stability in the water.^{52,53,66} Befitting its phylogenetic position, the whole-body COM of *Ichthyostega* is more anteriorly positioned than in any crown tetrapod studied herein, occupying a position intermediate between sarcopterygians and actinopterygians and lying closer to the shoulders than hips (Figure 3). This position reflects the unique body proportions of *Ichthyostega*, with forelimbs that are proportionally much larger than in other tetrapods (Figure 4A), thus exerting a much greater influence on whole-body COM position (Figure 4B). Considered together,

these results reveal a “front-heavy” body plan in which the forelimbs would have borne a higher fraction of body weight than the hindlimbs in a terrestrial setting. This greater extent of forelimb–substrate engagement and weight support thus reinforces the hypothesis of a forelimb-dominated mode of terrestrial locomotion in *Ichthyostega*,³³ irrespective of specific joint kinematics. Of further interest here, the body plan of *Ichthyostega* is most closely resembled among the crown tetrapods in our sample by the platypus, which, in conjunction with its relatively anteriorly-positioned COM (Figure 3), also has relatively massive forelimbs (Figure 4) that play a dominant role during aquatic locomotion.⁷⁴ Ultimately, further research involving analyses of musculoskeletal capacity in the generation and resistance of external environmental forces is necessary to explicitly test locomotor behaviors or capabilities in terrestrial versus aquatic environments, especially how the forelimbs might have acted in a propulsive versus weight support role (e.g.,^{34,45,50}).

A core aspect of aquatic locomotion into which our analyses can provide insight is body attitude at flotation equilibrium. Specifically, buoyancy is a key component of aquatic competence, having been used to assess aquatic tendencies or behaviors (e.g.,^{52,53,66,75}); body attitude in particular bears an important influence on the disposition of sensory systems (e.g., vision, especially in taxa with dorsally-placed orbits¹⁵) and ability to ventilate (e.g., in taxa with dorsally opening nares and/or spiracles¹³). Properties such as center-of-buoyancy (COB) and pitch angle may thus shed additional light on morphofunctional trends across the water-to-land transition. Remarkably, despite the major disparity in body shape, COM, and COB across our sample, we find that all taxa exhibit a relatively similar pitch at flotation equilibrium, mostly within 10° of each other (Figure 5). This uniformity suggests an intriguing scenario for stem tetrapods: if flotation attitude was relatively insensitive to transformations in body plan across the fish–tetrapod transition (as our results suggest), then this would have facilitated morphological evolution among stem tetrapods by eliminating a potential constraint on anatomical innovation. In other words, although some aspects of aquatic performance such as hydrodynamic streamlining or thrust generation would have been affected by changes to body proportions or overall body plan, the core competency to maintain a “neutral” position while buoyant—one in which the eyes and, in tetrapods, often the nostrils remain above the water’s surface^{13,15}—would not have been (Figure 5C). Stem tetrapods would therefore have been able to evolve novel body plans—such as the robust (Figure 2), front-heavy (Figure 3), and large-limbed (Figure 4) *Ichthyostega*—and thus explore segment configurations amenable to both terrestrial and aquatic modes of life.^{33,34,47,71,76} Such “evolutionary tinkering” has recently been highlighted in specific components of the tetrapod skeleton,⁴⁷ suggesting that the need to navigate these contrasting environments played a key role in driving innovation in the stem tetrapod body plan.

Altogether, our study sheds new light on the distinctive anatomy of *Ichthyostega*, further characterizing a unique body plan and mode of life not observed among extant fishes or tetrapods. Through deconstruction of the vertebrate body plan, we reveal that *Ichthyostega* combined traits of the “fish” body plan (namely, a front-heavy body construction; Figure 3) with what

became core aspects of the “crown tetrapod” body plan (namely, well-developed limbs and girdles; Figure 4). However, this combination was not accomplished by a simple linear transformation. Instead, these various features were combined and elaborated upon in a manner morphologically and functionally distinctive from either endpoint of the fish–tetrapod transition, resulting in a gestalt simultaneously intermediate between these two sides, yet strikingly different from both. When considering the seemingly contradictory picture of *Ichthyostega* as “intermediate-yet-unique” among vertebrates, it is tempting to focus on those aspects that differ—such as distinctive body proportions (Figure 4) and mode of locomotion³³—and thus dismiss *Ichthyostega* as simply an idiosyncratic offshoot during the early exploration of land. However, recognizing the prevalence of such innovation throughout the stem tetrapod body (e.g.,^{14,17,18,33,47,77,78}), we instead argue that this uniqueness is not an aberrance, but in fact a hallmark inherent to the complex transition from water to land. Collectively, these findings contribute to a renewed picture of early tetrapod evolution as a time of profound experimentation and diversification in morphology, function, and ecology.

Limitations of the study

Extinct taxa often have no directly comparable counterparts in the extant fauna,^{44,64} rendering deep-time transitions such as the origin of tetrapods difficult to analyze. Our taxon sample addresses this challenge by incorporating data from several extant taxa, none of which are “perfect” analogs on their own but which together capture a range of relevant ecologies, morphologies, and modes of locomotion while also providing phylogenetic context for *Ichthyostega*. By focusing on this set of analogs, our study therefore captures some of the body plans most relevant to contextualizing the mass properties of *Ichthyostega*.

As a methodological caveat, any soft-tissue reconstruction of this nature will bear inherent and unavoidable uncertainty, especially when analyzing fossils in which soft tissues are not preserved. To mitigate this uncertainty, we performed a variety of sensitivity analyses, testing the robustness of our results at each step of our overall analysis. Full details are provided in the [STAR Methods](#), but to summarize: (1) When constructing our models, we used the estimated paths of key appendicular musculature to constrain the dimensions of the proximal limb hoops, thus providing an anatomically informed basis for the “minimum” limb volumes (see “[muscle guidelines](#)”); (2) for the fossil specimens in our analysis, in which these muscles are not directly preserved, we used previous, phylogenetically informed reconstructions^{28,29} to identify these origin/insertion sites, taking a conservative approach when multiple muscle paths were possible (i.e., reconstructing every possible combination of origin/insertion) (see “[muscle guidelines](#)”); (3) given disagreements regarding limb proportions in prior reconstructions of *Ichthyostega*,^{7,17,33,54} we created additional variants of the hindlimb volumes for this taxon in order to test potential effects on mass properties (see “[further sensitivity analysis of Ichthyostega](#)”); and (4) in addition to using established protocols to determine the “minimum” and “maximum” plausible dimensions for each body segment,^{61,65} we more thoroughly estimated intraspecific variation by sampling mass property values from

between these bounds (see “assessment of intraspecific variation”).

Finally, regarding this latter point, our references to “intraspecific variation” also warrant a clear caveat. Each taxon is represented herein by the largest and/or best-preserved specimen currently available from CT scan data. A single adult or near-adult specimen can of course not provide a complete encapsulation of all intraspecific variation for a given taxon; to accomplish this, one would need to construct separate volumetric models for multiple specimens within that species. However, such an approach is often infeasible (hence the standard practice among volumetric mass reconstructions to only model a single “exemplar” specimen per taxon) or indeed impossible, especially for extinct taxa such as *Ichthyostega* for which few to no complete specimens exist. Therefore, although our population-based approach to calculating mass properties likely captures only a subset of the full range of intraspecific variation for each taxon, this technique nonetheless provides as thorough an estimation of this variation as reasonably possible given the available data. Supporting the utility of this approach, the range of mass properties recovered herein for *Eryops* and *Crocodylus* encapsulate the values derived by other studies from conspecific specimens (cf. Hart et al.⁶⁴ and Wright et al.,⁷⁹ respectively), indicating that our technique can indeed capture an informative approximation of intraspecific variation.

RESOURCE AVAILABILITY

Lead contact

Requests for further information and resources should be directed to and will be fulfilled by the lead contact, Catherine Strong (crstrong@g.harvard.edu).

Materials availability

The specimens examined as part of this study are accessioned and accessible through the museum collections in which they are housed (see [key resources table](#) for details). Meshes of each skeleton are provided in the Supplemental Information (Data S1), as are the volumetric models constructed for our analyses (Data S2–S3).

Data and code availability

- All data needed to evaluate the conclusions in this study are presented in the paper itself and/or the [Supplemental Information](#). All supplemental materials (Tables S1–S5, Code S1–S4, and Data S1–S4) are deposited in the Harvard Dataverse and are publicly available as of the date of publication at <https://doi.org/10.7910/DVN/JUMFW2>.
- All original code used for this study has been deposited in the Harvard Dataverse and is publicly available as of the date of publication at <https://doi.org/10.7910/DVN/JUMFW2>.
- Any additional information required to reanalyze the data reported in this paper is available from the [lead contact](#) upon request.

ACKNOWLEDGMENTS

We thank Pierce Lab members for helpful discussions during project development, especially Mark Wright for suggestions and inspiration regarding our analyses of buoyancy-related properties. We also thank the anonymous reviewers who provided valuable feedback on previous versions of this manuscript. Finally, additional thanks are extended to the late Jenny Clack whose work on early tetrapod evolution inspired the present study.

This research was supported by the Natural Sciences and Engineering Research Council of Canada (Postgraduate Scholarship–Doctoral, awarded to C.R.C.S.), the Department of Organismic and Evolutionary Biology at Harvard University (Robert A. Chapman Memorial Scholarship, awarded to C.R.

C.S.), the United States National Science Foundation (grant no EAR-2122115, awarded to S.E.P.), and the United Kingdom Natural Environment Research Council (grant nos NE/G00711X/1 and NE/K004751/1, awarded to J.R.H. and S.E.P.).

Sources regarding CT scan data are provided in the [key resources table](#). Certain scans used in this study were downloaded from MorphoSource, Duke University (see [key resources table](#)), and were accompanied by the following attribution statements. The scan for *Amia calva* (UF F-236194) was provided by the Florida Museum of Natural History, University of Florida, with funding from oVert TCN and NSF DBI-1701714. Katharine Criswell provided access to the data for *Neoceratodus forsteri* (AM I-40438-001), with data collection funded by NSF EAR-0646848 and data upload to MorphoSource funded by DBI-1902242. Thomas Stewart et al. provided access to the data for *Neoceratodus forsteri* (MCZ I-157440), originally appearing in Stewart et al.,⁸⁰ with funding provided via the Brinson Foundation and the National Science Foundation (EAR 0207721, EAR 0544093, EAR 0208733, EAR 0544565). Finally, the scan data for *Ambystoma tigrinum* (TNHC 17991) are available on DigiMorph. This specimen was made available to The University of Texas High-Resolution X-ray CT Facility by Dr. Timothy Rowe of The University of Texas at Austin. Funding for scanning was provided by a National Science Foundation Assembling the Tree of Life grant to Dr. Rowe. Funding for image processing was provided by a National Science Foundation Digital Libraries Initiative grant to Dr. Rowe.

AUTHOR CONTRIBUTIONS

Conceptualization: all authors; data curation: C.R.C.S., P.J.B., and S.E.P.; formal analysis: C.R.C.S. and P.J.B.; funding acquisition: C.R.C.S., J.R.H., and S.E.P.; investigation: C.R.C.S. and P.J.B.; methodology: C.R.C.S., P.J.B., and S.E.P.; project administration: C.R.C.S., P.J.B., and S.E.P.; software: C.R.C.S. and P.J.B.; resources: J.R.H. and S.E.P.; supervision: S.E.P.; visualization: C.R.C.S., P.J.B., and S.E.P.; writing—original draft: C.R.C.S., P.J.B., and S.E.P.; writing—review and editing: all authors.

DECLARATION OF INTERESTS

The authors declare no competing interests.

STAR★METHODS

Detailed methods are provided in the online version of this paper and include the following:

- [KEY RESOURCES TABLE](#)
- [EXPERIMENTAL MODEL AND STUDY PARTICIPANT DETAILS](#)
 - Taxon sample
- [METHOD DETAILS](#)
 - Model preparation
 - Model construction
 - Model finalization
 - Further sensitivity analysis of *Ichthyostega*
- [QUANTIFICATION AND STATISTICAL ANALYSIS](#)
 - Analysis of mass properties
 - Analysis of flotation equilibrium
 - Data processing and visualization

SUPPLEMENTAL INFORMATION

Supplemental information can be found online at <https://doi.org/10.1016/j.isci.2025.112486>.

Received: November 27, 2024

Revised: March 14, 2025

Accepted: April 16, 2025

Published: April 19, 2025

REFERENCES

- Clack, J.A. (2012). *Gaining Ground: The Origin and Evolution of Tetrapods*, 2nd Edition (Indiana University Press).
- Ahlberg, P.E. (2018). Follow the footprints and mind the gaps: a new look at the origin of tetrapods. *Earth Environ. Sci. Trans. R. Soc. Edinb.* 109, 115–137. <https://doi.org/10.1017/S1755691018000695>.
- Coates, M.I., and Clack, J.A. (1990). Polydactyly in the earliest known tetrapod limbs. *Nature* 347, 66–69. <https://doi.org/10.1038/347066a0>.
- Coates, M.I. (1996). The Devonian tetrapod *Acanthostega gunnari* Jarvik: postcranial anatomy, basal tetrapod interrelationships and patterns of skeletal evolution. *Trans. R. Soc. Edinb. Earth Sci.* 87, 363–421. <https://doi.org/10.1017/S0263593300006787>.
- Clack, J.A. (2005). Getting a leg up on land. *Sci. Am.* 293, 100–107.
- Niedźwiedzki, G., Szrek, P., Narkiewicz, K., Narkiewicz, M., and Ahlberg, P.E. (2010). Tetrapod trackways from the early Middle Devonian period of Poland. *Nature* 463, 43–48. <https://doi.org/10.1038/nature08623>.
- Jarvik, E. (1980). *Basic Structure and Evolution of the Vertebrates* (Academic Press).
- Ahlberg, P.E., and Clack, J.A. (1998). Lower jaws, lower tetrapods—a review based on the Devonian genus *Acanthostega*. *Trans. R. Soc. Edinb. Earth Sci.* 89, 11–46. <https://doi.org/10.1017/S0263593300002340>.
- Ahlberg, P.E., Clack, J.A., Lukševičs, E., Blom, H., and Zupiņš, I. (2008). *Ventastega curonica* and the origin of tetrapod morphology. *Nature* 453, 1199–1204. <https://doi.org/10.1038/nature06991>.
- Downs, J.P., Daeschler, E.B., Jenkins, F.A., Jr., and Shubin, N.H. (2008). The cranial endoskeleton of *Tiktaalik roseae*. *Nature* 455, 925–929. <https://doi.org/10.1038/nature07189>.
- Markey, M.J., and Marshall, C.R. (2007). Terrestrial-style feeding in a very early aquatic tetrapod is supported by evidence from experimental analysis of suture morphology. *Proc. Natl. Acad. Sci. USA* 104, 7134–7138. <https://doi.org/10.1073/pnas.0701706104>.
- Lemberg, J.B., Daeschler, E.B., and Shubin, N.H. (2021). The feeding system of *Tiktaalik roseae*: an intermediate between suction feeding and biting. *Proc. Natl. Acad. Sci. USA* 118, e2016421118. <https://doi.org/10.1073/pnas.2016421118>.
- Clack, J.A. (2007). Devonian climate change, breathing, and the origin of the tetrapod stem group. *Integr. Comp. Biol.* 47, 510–523. <https://doi.org/10.1093/icb/pcm055>.
- Clack, J.A., Ahlberg, P.E., Finney, S.M., Dominguez Alonso, P., Robinson, J., and Ketcham, R.A. (2003). A uniquely specialized ear in a very early tetrapod. *Nature* 425, 65–69. <https://doi.org/10.1038/nature01904>.
- Maclver, M.A., Schmitz, L., Mugan, U., Murphey, T.D., and Mobley, C.D. (2017). Massive increase in visual range preceded the origin of terrestrial vertebrates. *Proc. Natl. Acad. Sci. USA* 114, E2375–E2384. <https://doi.org/10.1073/pnas.1615563114>.
- Daeschler, E.B., Shubin, N.H., and Jenkins, F.A., Jr. (2006). A Devonian tetrapod-like fish and the evolution of the tetrapod body plan. *Nature* 440, 757–763. <https://doi.org/10.1038/nature04639>.
- Ahlberg, P.E., Clack, J.A., and Blom, H. (2005). The axial skeleton of the Devonian tetrapod *Ichthyostega*. *Nature* 437, 137–140. <https://doi.org/10.1038/nature03893>.
- Pierce, S.E., Ahlberg, P.E., Hutchinson, J.R., Molnar, J.L., Sanchez, S., Tafforeau, P., and Clack, J.A. (2013). Vertebral architecture in the earliest stem tetrapods. *Nature* 494, 226–229. <https://doi.org/10.1038/nature11825>.
- Stewart, T.A., Lemberg, J.B., Hillan, E.J., Magallanes, I., Daeschler, E.B., and Shubin, N.H. (2024). The axial skeleton of *Tiktaalik roseae*. *Proc. Natl. Acad. Sci. USA* 121, e2316106121. <https://doi.org/10.1073/pnas.2316106121>.
- Coates, M.I., Jeffery, J.E., and Rut, M. (2002). Fins to limbs: what the fossils say. *Evol. Dev.* 4, 390–401. <https://doi.org/10.1046/j.1525-142X.2002.02026.x>.
- Shubin, N.H., Daeschler, E.B., and Jenkins, F.A., Jr. (2006). The pectoral fin of *Tiktaalik roseae* and the origin of the tetrapod limb. *Nature* 440, 764–771. <https://doi.org/10.1038/nature04637>.
- Ahlberg, P.E. (2011). Humeral homology and the origin of the tetrapod elbow: a reinterpretation of the enigmatic specimens ANSP 21350 and GSM 104536. *Spec. Pap. Palaeontol.* 86, 17–29. <https://doi.org/10.1111/j.1475-4983.2011.01077.x>.
- Esteve-Altava, B., Pierce, S.E., Molnar, J.L., Johnston, P., Diogo, R., and Hutchinson, J.R. (2019). Evolutionary parallels of pectoral and pelvic network-anatomy from fins to limbs. *Sci. Adv.* 5, eaau7459. <https://doi.org/10.1126/sciadv.aau7459>.
- Boisvert, C.A., Mark-Kurik, E., and Ahlberg, P.E. (2008). The pectoral fin of *Panderichthys* and the origin of digits. *Nature* 456, 636–638. <https://doi.org/10.1038/nature07339>.
- Cloutier, R., Clement, A.M., Lee, M.S.Y., Noël, R., Béchar, I., Roy, V., and Long, J.A. (2020). *Elpistostege* and the origin of the vertebrate hand. *Nature* 579, 549–554. <https://doi.org/10.1038/s41586-020-2100-8>.
- Bishop, P.J. (2014). The humerus of *Ossinodus pueri*, a stem tetrapod from the Carboniferous of Gondwana, and the early evolution of the tetrapod forelimb. *Alcheringa* 38, 209–238. <https://doi.org/10.1080/03115518.2014.861320>.
- Esteve-Altava, B., Molnar, J.L., Johnston, P., Hutchinson, J.R., and Diogo, R. (2018). Anatomical network analysis of the musculoskeletal system reveals integration loss and parcellation boost during the fins-to-limbs transition. *Evolution* 72, 601–618. <https://doi.org/10.1111/evo.13430>.
- Molnar, J.L., Diogo, R., Hutchinson, J.R., and Pierce, S.E. (2018). Reconstructing pectoral appendicular muscle anatomy in fossil fish and tetrapods over the fins-to-limbs transition. *Biol. Rev.* 93, 1077–1107. <https://doi.org/10.1111/brv.12386>.
- Molnar, J.L., Diogo, R., Hutchinson, J.R., and Pierce, S.E. (2020). Evolution of hindlimb muscle anatomy across the tetrapod water-to-land transition, including comparisons with forelimb anatomy. *Anat. Rec.* 303, 218–234. <https://doi.org/10.1002/ar.23997>.
- Vogel, S. (2003). *Comparative Biomechanics: Life's Physical World* (Princeton University Press).
- Biewener, A.A., and Patek, S.N. (2018). *Animal Locomotion*, 2 Edition (Oxford University Press).
- Nyakatura, J.A., Andrada, E., Curth, S., and Fischer, M.S. (2014). Bridging “Romer’s Gap”: limb mechanics of an extant belly-dragging lizard inform debate on tetrapod locomotion during the Early Carboniferous. *Evol. Biol.* 41, 175–190. <https://doi.org/10.1007/s11692-013-9266-z>.
- Pierce, S.E., Clack, J.A., and Hutchinson, J.R. (2012). Three-dimensional limb joint mobility in the early tetrapod *Ichthyostega*. *Nature* 486, 523–526. <https://doi.org/10.1038/nature11124>.
- Molnar, J.L., Hutchinson, J.R., Diogo, R., Clack, J.A., and Pierce, S.E. (2021). Evolution of forelimb musculoskeletal function across the fish-to-tetrapod transition. *Sci. Adv.* 7, eabd7457. <https://doi.org/10.1126/sciadv.abd7457>.
- Hildebrand, M. (1966). Analysis of the symmetrical gaits of tetrapods. *Folia Biotheoretica* 6, 9–22.
- McElroy, E.J., and Granatosky, M.C. (2022). The evolution of asymmetrical gaits in gnathostome vertebrates. *J. Exp. Biol.* 225, jeb243235. <https://doi.org/10.1242/jeb.243235>.
- Edwards, J.L. (1977). The evolution of terrestrial locomotion. In *Major Patterns in Vertebrate Evolution*, M.K. Hecht, P.C. Goody, and B.M. Hecht, eds. (Springer), pp. 553–577. <https://doi.org/10.1007/978-1-4684-8851-7>.
- Frolich, L.M., and Biewener, A.A. (1992). Kinematic and electromyographic analysis of the functional role of the body axis during terrestrial and aquatic locomotion in the salamander *Ambystoma tigrinum*. *J. Exp. Biol.* 162, 107–130. <https://doi.org/10.1242/jeb.162.1.107>.
- Ashley-Ross, M. (1994). Hindlimb kinematics during terrestrial locomotion in a salamander (*Dicamptodon tenebrosus*). *J. Exp. Biol.* 193, 255–283. <https://doi.org/10.1242/jeb.193.1.255>.

40. Boisvert, C.A. (2005). The pelvic fin and girdle of *Panderichthys* and the origin of tetrapod locomotion. *Nature* 438, 1145–1147. <https://doi.org/10.1038/nature04119>.
41. King, H.M., Shubin, N.H., Coates, M.I., and Hale, M.E. (2011). Behavioral evidence for the evolution of walking and bounding before terrestriality in sarcopterygian fishes. *Proc. Natl. Acad. Sci. USA* 108, 21146–21151. <https://doi.org/10.1073/pnas.1118669109>.
42. Kawano, S.M., and Blob, R.W. (2013). Propulsive forces of mudskipper fins and salamander limbs during terrestrial locomotion: implications for the invasion of land. *Integr. Comp. Biol.* 53, 283–294. <https://doi.org/10.1093/icb/ict051>.
43. Pridmore, P. (1994). Submerged walking in the epaulette shark *Hemiscyllium ocellatum* (Hemiscyllidae) and its implications for locomotion in rhipidistian fishes and early tetrapods. *Zoology* 98, 278–297.
44. Pierce, S.E., Hutchinson, J.R., and Clack, J.A. (2013). Historical perspectives on the evolution of tetrapodomorph movement. *Integr. Comp. Biol.* 53, 209–223. <https://doi.org/10.1093/icb/ict022>.
45. Bishop, P.J., Cuff, A.R., and Hutchinson, J.R. (2021). How to build a dinosaur: musculoskeletal modeling and simulation of locomotor biomechanics in extinct animals. *Paleobiology* 47, 1–38. <https://doi.org/10.1017/pab.2020.46>.
46. Neenan, J.M., Ruta, M., Clack, J.A., and Rayfield, E.J. (2014). Feeding biomechanics in *Acanthostega* and across the fish–tetrapod transition. *Proc. Biol. Sci.* 281, 20132689. <https://doi.org/10.1098/rspb.2013.2689>.
47. Dickson, B.V., Clack, J.A., Smithson, T.R., and Pierce, S.E. (2021). Functional adaptive landscapes predict terrestrial capacity at the origin of limbs. *Nature* 589, 242–245. <https://doi.org/10.1038/s41586-020-2974-5>.
48. Alexander, R.M. (1985). Body support, scaling, and allometry. In *Functional Vertebrate Morphology*, M. Hildebrand, D.M. Bramble, K.F. Liem, and D.B. Wake, eds. (Harvard University Press), pp. 26–37.
49. Pandy, M.G., Kumar, V., Berme, N., and Waldron, K.J. (1988). The dynamics of quadrupedal locomotion. *J. Biomech. Eng.* 110, 230–237. <https://doi.org/10.1115/1.3108436>.
50. Kawano, S.M., and Blob, R.W. (2022). Terrestrial force production by the limbs of a semi-aquatic salamander provides insight into the evolution of terrestrial locomotor mechanics. *J. Exp. Biol.* 225, jeb242795. <https://doi.org/10.1242/jeb.242795>.
51. Cieri, R.L., Dick, T.J.M., Irwin, R., Rumsey, D., and Clemente, C.J. (2021). The scaling of ground reaction forces and duty factor in monitor lizards: implications for locomotion in sprawling tetrapods. *Biol. Lett.* 17, 20200612. <https://doi.org/10.1098/rsbl.2020.0612>.
52. Henderson, D.M. (2003). Effects of stomach stones on the buoyancy and equilibrium of a floating crocodylian: a computational analysis. *Can. J. Zool.* 81, 1346–1357. <https://doi.org/10.1139/Z03-122>.
53. Henderson, D.M. (2004). Tippy punters: sauropod dinosaur pneumaticity, buoyancy and aquatic habits. *Proc. Biol. Sci.* 271, S180–S183. <https://doi.org/10.1098/rsbl.2003.0136>.
54. Jarvik, E. (1996). The Devonian tetrapod *Ichthyostega*. *Lethaia* 29, 76–206.
55. Clack, J.A. (2006). The emergence of early tetrapods. *Palaeogeogr. Palaeoclimatol. Palaeoecol.* 232, 167–189. <https://doi.org/10.1016/j.palaeo.2005.07.019>.
56. Clack, J.A. (2009). The fin to limb transition: new data, interpretations, and hypotheses from paleontology and developmental biology. *Annu. Rev. Earth Planet Sci.* 37, 163–179. <https://doi.org/10.1146/annurev.earth.36.031207.124146>.
57. Callier, V., Clack, J.A., and Ahlberg, P.E. (2009). Contrasting developmental trajectories in the earliest known tetrapod forelimbs. *Science* 324, 364–367. <https://doi.org/10.1126/science.1167542>.
58. Carroll, R.L., Irwin, J., and Green, D.M. (2005). Thermal physiology and the origin of terrestriality in vertebrates. *Zool. J. Linn. Soc.* 143, 345–358. <https://doi.org/10.1111/j.1096-3642.2005.00151.x>.
59. Clack, J.A. (2005). Making headway and finding a foothold: tetrapods come ashore. In *Evolving Form and Function: Fossils and Development*, G. Briggs, ed. (Peabody Museum of Natural History), pp. 223–244.
60. Henderson, D.M. (1999). Estimating the masses and centers of mass of extinct animals by 3-D mathematical slicing. *Paleobiology* 25, 88–106. [https://doi.org/10.1666/0094-8373\(1999\)025<0088:ETMACO>2.3.CO;2](https://doi.org/10.1666/0094-8373(1999)025<0088:ETMACO>2.3.CO;2).
61. Allen, V., Paxton, H., and Hutchinson, J.R. (2009). Variation in center of mass estimates for extant sauropsids and its importance for reconstructing inertial properties of extinct archosaurs. *Anat. Rec.* 292, 1442–1461. <https://doi.org/10.1002/ar.20973>.
62. Brassey, C.A. (2017). Body-mass estimation in paleontology: a review of volumetric techniques. *Paleontol. Soc. Pap.* 22, 133–156. <https://doi.org/10.1017/scs.2017.12>.
63. Nyakatura, J.A., Allen, V.R., Lauster, J., Andikfar, A., Danczak, M., Ullrich, H.-J., Hufenbach, W., Martens, T., and Fischer, M.S. (2015). A three-dimensional skeletal reconstruction of the stem amniote *Orobates pabsti* (Diadectidae): analyses of body mass, centre of mass position, and joint mobility. *PLoS One* 10, e0137284. <https://doi.org/10.1371/journal.pone.0137284>.
64. Hart, L.J., Campione, N.E., and McCurry, M.R. (2022). On the estimation of body mass in temnospondyls: a case study using the large-bodied *Eryops* and *Paracyclotossaurus*. *Palaeontology* 65, e12629. <https://doi.org/10.1111/pala.12629>.
65. Allen, V., Bates, K.T., Li, Z., and Hutchinson, J.R. (2013). Linking the evolution of body shape and locomotor biomechanics in bird-line archosaurs. *Nature* 497, 104–107. <https://doi.org/10.1038/nature12059>.
66. Henderson, D.M. (2006). Floating point: a computational study of buoyancy, equilibrium, and gastroliths in plesiosaurs. *Lethaia* 39, 227–244. <https://doi.org/10.1080/00241160600799846>.
67. Deyst, K.A., and Liem, K.F. (1985). The muscular basis of aerial ventilation of the primitive lung of *Amia calva*. *Respir. Physiol.* 59, 213–223. [https://doi.org/10.1016/0034-5687\(85\)90008-8](https://doi.org/10.1016/0034-5687(85)90008-8).
68. Anderson, P.S.L., Friedman, M., and Ruta, M. (2013). Late to the table: diversification of tetrapod mandibular biomechanics lagged behind the evolution of terrestriality. *Integr. Comp. Biol.* 53, 197–208. <https://doi.org/10.1093/icb/ict006>.
69. Deakin, W.J., Anderson, P.S.L., den Boer, W., Smith, T.J., Hill, J.J., Rücklin, M., Donoghue, P.C.J., and Rayfield, E.J. (2022). Increasing morphological disparity and decreasing optimality for jaw speed and strength during the radiation of jawed vertebrates. *Sci. Adv.* 8, eab3644. <https://doi.org/10.1126/sciadv.ab3644>.
70. Simões, T.R., and Pierce, S.E. (2021). Sustained high rates of morphological evolution during the rise of tetrapods. *Nat. Ecol. Evol.* 5, 1403–1414. <https://doi.org/10.1038/s41559-021-01532-x>.
71. Rawson, J.R.G., Esteve-Altava, B., Porro, L.B., Dutel, H., and Rayfield, E. J. (2022). Early tetrapod cranial evolution is characterized by increased complexity, constraint, and an offset from fin–limb evolution. *Sci. Adv.* 8, eadc8875. <https://doi.org/10.1126/sciadv.adc8875>.
72. Ruta, M., and Wills, M.A. (2016). Comparable disparity in the appendicular skeleton across the fish–tetrapod transition, and the morphological gap between fish and tetrapod postcrania. *Palaeontology* 59, 249–267. <https://doi.org/10.1111/pala.12227>.
73. Macesic, L.J., and Kajiura, S.M. (2010). Comparative punting kinematics and pelvic fin musculature of benthic batoids. *J. Morphol.* 271, 1219–1228. <https://doi.org/10.1002/jmor.10865>.
74. Howell, A.B. (1937). The swimming mechanism of the platypus. *J. Mammal.* 18, 217–222. <https://doi.org/10.2307/1374471>.
75. Henderson, D.M. (2018). A buoyancy, balance and stability challenge to the hypothesis of a semi-aquatic *Spinosaurus* Stromer, 1915 (Dinosauria: Theropoda). *PeerJ* 6, e5409. <https://doi.org/10.7717/peerj.5409>.
76. Otoo, B.K.A., Bolt, J.R., Lombard, R.E., Angielczyk, K.D., and Coates, M.I. (2021). The postcranial anatomy of *Whatcheeria deltae* and its implications

- for the family Whatcheeridae. *Zool. J. Linn. Soc.* 193, 700–745. <https://doi.org/10.1093/zoolinnean/zlaa182>.
77. Pardo, J.D., Szostakiwskyj, M., Ahlberg, P.E., and Anderson, J.S. (2017). Hidden morphological diversity among early tetrapods. *Nature* 546, 642–645. <https://doi.org/10.1038/nature22966>.
 78. Beznosov, P.A., Clack, J.A., Lukševičs, E., Ruta, M., and Ahlberg, P.E. (2019). Morphology of the earliest reconstructable tetrapod *Parmastega aelidae*. *Nature* 574, 527–531. <https://doi.org/10.1038/s41586-019-1636-y>.
 79. Wright, M.A., Cavanaugh, T.J., and Pierce, S.E. (2024). Volumetric versus element-scaling mass estimation and its application to Permo-Triassic tetrapods. *Integr. Org. Biol.* 6, obae034. <https://doi.org/10.1093/iob/obae034>.
 80. Stewart, T.A., Lemberg, J.B., Taft, N.K., Yoo, I., Daeschler, E.B., and Shubin, N.H. (2020). Fin ray patterns at the fin-to-limb transition. *Proc. Natl. Acad. Sci. USA* 117, 1612–1620. <https://doi.org/10.1073/pnas.1915983117>.
 81. Miner, R.W. (1925). The pectoral limb of *Eryops* and other primitive tetrapods. *Bull. Am. Mus. Nat. Hist.* 51, 145–312.
 82. Pawley, K., and Warren, A. (2006). The appendicular skeleton of *Eryops megacephalus* Cope, 1877 (Temnospondyli: Eryopoidea) from the Lower Permian of North America. *J. Paleontol.* 80, 561–580. [https://doi.org/10.1666/0022-3360\(2006\)80\[561:TASOEM\]2.0.CO;2](https://doi.org/10.1666/0022-3360(2006)80[561:TASOEM]2.0.CO;2).
 83. Herbst, E.C., Manafzadeh, A.R., and Hutchinson, J.R. (2022). Multi-joint analysis of pose viability supports the possibility of salamander-like hindlimb configurations in the Permian tetrapod *Eryops megacephalus*. *Integr. Comp. Biol.* 62, 139–151. <https://doi.org/10.1093/icb/icac083>.
 84. Bishop, P.J., Bates, K.T., Allen, V.R., Henderson, D.M., Randau, M., and Hutchinson, J.R. (2020). Relationships of mass properties and body proportions to locomotor habit in terrestrial Archosauria. *Paleobiology* 46, 550–568. <https://doi.org/10.1017/pab.2020.47>.
 85. Lebedev, O.A., and Coates, M.I. (1995). The postcranial skeleton of the Devonian tetrapod *Tulerpeton curtum* Lebedev. *Zool. J. Linn. Soc.* 114, 307–348. <https://doi.org/10.1111/j.1096-3642.1995.tb00119.x>.
 86. Yamanoue, Y., Setiamarga, D.H.E., and Matsuura, K. (2010). Pelvic fins in teleosts: structure, function and evolution. *J. Fish. Biol.* 77, 1173–1208. <https://doi.org/10.1111/j.1095-8649.2010.02674.x>.
 87. Böhmer, C., Theil, J.-C., Fabre, A.-C., and Herrel, A. (2020). *Atlas of Terrestrial Mammal Limbs* (CRC Press).
 88. Klinkhamer, A.J., Wilhite, D.R., White, M.A., and Wroe, S. (2017). Digital dissection and three-dimensional interactive models of limb musculature in the Australian estuarine crocodile (*Crocodylus porosus*). *PLoS One* 12, e0175079. <https://doi.org/10.1371/journal.pone.0175079>.
 89. Meers, M.B. (2003). Crocodylian forelimb musculature and its relevance to Archosauria. *Anat. Rec.* 274, 891–916. <https://doi.org/10.1002/ar.a.10097>.
 90. Walthall, J.C., and Ashley-Ross, M.A. (2006). Postcranial myology of the California newt, *Taricha torosa*. *Anat. Rec.* 288, 46–57. <https://doi.org/10.1002/ar.a.20279>.
 91. Otero, A., Bishop, P.J., and Hutchinson, J.R. (2024). Hindlimb biomechanics of *Lagosuchus talampayensis* (Archosauria, Dinosauriformes), with comments on skeletal morphology. *J. Anat.* 00, 1–26. <https://doi.org/10.1111/joa.14183>.
 92. Motani, R. (2001). Estimating body mass from silhouettes: testing the assumption of elliptical body cross-sections. *Paleobiology* 27, 735–750. [https://doi.org/10.1666/00948373\(2001\)027<0735:EBMFST>2.0.CO;2](https://doi.org/10.1666/00948373(2001)027<0735:EBMFST>2.0.CO;2).
 93. Gonzales, T.T., Kato, M., Ghaffar, M.A., and Ishimatsu, A. (2011). Gross and fine anatomy of the respiratory vasculature of the mudskipper, *Periophthalmodon schlosseri* (Gobiidae: Oxudercinae). *J. Morphol.* 272, 629–640. <https://doi.org/10.1002/jmor.10944>.
 94. Grigg, G.C. (1965). Studies on the Queensland Lungfish, *Neoceratodus forsteri* (Kreffl). I. Anatomy, histology, and functioning of the lung. *Aust. J. Zool.* 13, 243–254. <https://doi.org/10.1071/ZO9650243>.
 95. Brainerd, E.L. (1998). Mechanics of lung ventilation in a larval salamander *Ambystoma tigrinum*. *J. Exp. Biol.* 201, 2891–2901. <https://doi.org/10.1242/jeb.201.20.2891>.
 96. Macaulay, S., Hutchinson, J.R., and Bates, K.T. (2017). A quantitative evaluation of physical and digital approaches to centre of mass estimation. *J. Anat.* 231, 758–775. <https://doi.org/10.1111/joa.12667>.
 97. Larramendi, A., Paul, G.S., and Hsu, S.-Y. (2021). A review and reappraisal of the specific gravities of present and past multicellular organisms, with an emphasis on tetrapods. *Anat. Rec.* 304, 1833–1888. <https://doi.org/10.1002/ar.24574>.
 98. R Core Team (2023). *R: A Language and Environment for Statistical Computing* (R Foundation for Statistical Computing).
 99. Posit team (2024). *RStudio: Integrated Development Environment for R* (Posit Software PBC).

STAR★METHODS

KEY RESOURCES TABLE

REAGENT or RESOURCE	SOURCE	IDENTIFIER
Biological samples		
<i>Amia calva</i>	Florida Museum of Natural History, University of Florida	UF F-236194
<i>Ambystoma tigrinum</i>	Texas Natural History Collections, University of Texas at Austin	TNHC 17991
<i>Crocodylus moreletii</i>	Royal Veterinary College	RVC-JRH-FMC2
<i>Eryops megacephalus</i>	Museum of Comparative Zoology, Harvard University	MCZ VPRA-1539
<i>Halichoerus grypus</i>	University Museum of Zoology, Cambridge University	UMZC K.7943
<i>Ichthyostega</i> sp.	Geological Museum, Natural History Museum of Denmark	Composite of several MGUH VP specimens (1349, 6012, 6039, 6064, 6077, 6079, 6093, 6098, 6109, 6115, 6132, 6140, 6146, 6154, 6167, 6250, 29017); see Pierce et al. 2012 ³³ for details.
<i>Lutra vulgaris</i>	University Museum of Zoology, Cambridge University	UMZC K.2768
<i>Neoceratodus forsteri</i>	Australian Museum	AM I-40438-001
<i>Neoceratodus forsteri</i>	Museum of Comparative Zoology, Harvard University	MCZ I-157440
<i>Ornithorhynchus anatinus</i>	National Museum of Natural History, Smithsonian Institution	USNM 221110
<i>Periophthalmodon freycineti</i>	Florida Museum of Natural History, University of Florida	UF F-117163
Deposited data		
Downsampled skeleton meshes of all specimens	This paper; Harvard Dataverse	Data S1; https://doi.org/10.7910/DVN/JUMFW2
Volumetric segment meshes for all models	This paper; Harvard Dataverse	Data S2; https://doi.org/10.7910/DVN/JUMFW2
Whole-body buoyancy meshes for all models	This paper; Harvard Dataverse	Data S3; https://doi.org/10.7910/DVN/JUMFW2
Raw results from Code S1 and S2	This paper; Harvard Dataverse	Data S4; https://doi.org/10.7910/DVN/JUMFW2
MicroCT scan of <i>Amia calva</i>	MorphoSource	ark:/87602/m4/384858
MicroCT scan of <i>Ambystoma tigrinum</i>	DigiMorph	https://digimorph.org/specimens/Ambystoma_tigrinum/whole/
MicroCT scan of <i>Crocodylus moreletii</i>	CrocBase	https://osf.io/x38nh/
MicroCT scan of AM <i>Neoceratodus forsteri</i>	MorphoSource	ark:/87602/m4/M115978
MicroCT scan of MCZ <i>Neoceratodus forsteri</i>	MorphoSource	ark:/87602/m4/M97859
Mesh of MCZ <i>Neoceratodus forsteri</i>	Sketchfab	https://sketchfab.com/3d-models/australian-lungfish-pectoral-fin-endoskeleton-73b42496d3ad4d218e4fd49a21019135
MicroCT scan of <i>Periophthalmodon freycineti</i>	MorphoSource	ark:/87602/m4/499413
Software and algorithms		
MATLAB code for calculating mass properties using a population-based approach	This paper; Harvard Dataverse	Code S1; https://doi.org/10.7910/DVN/JUMFW2
MATLAB code for conducting simulations of flotational equilibrium	This paper; Harvard Dataverse	Code S2; https://doi.org/10.7910/DVN/JUMFW2
MATLAB code for calculating the mass properties of every possible combination of maximum versus minimum segments for each taxon	This paper; Harvard Dataverse	Code S3; https://doi.org/10.7910/DVN/JUMFW2

(Continued on next page)

Continued

REAGENT or RESOURCE	SOURCE	IDENTIFIER
R script for processing and visualizing data	This paper; Harvard Dataverse	Code S4; https://doi.org/10.7910/DVN/JUMFW2
MorphoSource	Duke University	RRID: SCR_025654; https://www.morphosource.org/
Sketchfab	Sketchfab	https://sketchfab.com/
Mimics (v.22.0)	Materialise	RRID: SCR_012153; https://www.materialise.com/en/healthcare/mimics-innovation-suite/mimics
3-matic (v.17.0)	Materialise	https://www.materialise.com/en/industrial/software/3-matic
Rhinoceros 3D (v.7.SR36)	Robert McNeel & Associates	RRID: SCR_014339; https://www.rhino3d.com/
MATLAB (v.R2023b)	MathWorks	RRID: SCR_001622; https://www.mathworks.com/products/matlab.html
R (v.4.3.2)	R Core Team	RRID: SCR_001905; https://www.r-project.org/
RStudio (v.2023.12.1.402)	Posit Team	RRID:SCR_000432; https://posit.co/download/rstudio-desktop/

EXPERIMENTAL MODEL AND STUDY PARTICIPANT DETAILS

Taxon sample

To provide a comparative framework for interpreting the mass properties of *Ichthyostega*, we modeled it alongside eight extant taxa (Figures 1A, S2, and S3): *Ambystoma tigrinum* (tiger salamander), *Amia calva* (bowfin), *Crocodylus moreletii* (Morelet's crocodile), *Halichoerus grypus* (gray seal), *Lutra vulgaris* (Eurasian otter), *Neoceratodus forsteri* (Australian lungfish), *Ornithorhynchus anatinus* (platypus), and *Periophthalmodon freycineti* (pug-headed mudskipper). Beyond phylogenetically bracketing the fish–tetrapod transition, these taxa collectively encompass a range of ‘fish’ and semi-aquatic ‘tetrapod’ body plans and lifestyles, which have been variously inferred to represent functional or ecological analogs for stem tetrapods.⁴⁴ As another point of reference, we also modeled the early Permian stem amphibian *Eryops megacephalus*, given the widely regarded terrestrial competence of this taxon.^{81–83} Digital models of the skeletons of the seven tetrapods had been generated in prior studies,^{33,79,84} whereas the skeletal models of the three fishes were constructed using data from MorphoSource (RRID: SCR_025654) and Sketchfab, with microCT segmentation performed in Mimics (Materialise, v.22.0; RRID: SCR_012153) (see [key resources table](#)). In addition to skeletal geometry, *in situ* geometry of the flesh was also available for the *Crocodylus moreletii* specimen,⁸⁴ permitting a direct comparison between estimated and known soft-tissue volumes for this taxon and a test of our approach to body mass modeling.

METHOD DETAILS

Model preparation

Specimen completeness

Complete skeletal models of the taxa used in this study had either been generated in previous work (the six crown tetrapods^{33,79,84}) or were constructed based on whole-skeleton microCT data (*Amia* and *Periophthalmodon*) (see [key resources table](#)). However, the remaining two taxa were both incomplete: *Ichthyostega*³³ lacks preserved metacarpals, manual phalanges, and most of the carpals, and no scans or models of the complete skeleton of *Neoceratodus* were available online.

For *Ichthyostega*, addressing this absence was relatively minor: First, we constructed hoops (see also “[model construction](#)” below) along as much of the forelimb as possible (i.e., along the stylopod and zeugopod, ending at the proximal extent of the wrist). We then completed the remainder of the forelimb using a copy of the hoops constructed for the ankle and pedal digits, scaling these to match the dimensions of the aforementioned ‘proximal wrist’ hoop. This approach assumes that the manus and pes were similar to one another in gross dimensions, which is supported by other Devonian taxa.^{4,85}

For *Neoceratodus*, we assembled the skeleton of this taxon by combining two specimens (see also [key resources table](#)): AM I-40438-001 (whole-body skeleton, except fins and pelvic girdle) and MCZ I-157440 (right pectoral fin and girdle). To combine the fin of MCZ I-157440 with the body of AM I-40438-001, we digitally segmented the pectoral girdle, scapulocoracoid, and humerus from the MCZ specimen's microCT scan, and scaled these to match the size and placement of the corresponding elements in the AM specimen. We then added a pre-segmented mesh of the MCZ fin (created by Stewart et al.⁸⁰) by aligning it to the dimensions of the humerus. Finally, we mirrored this right fin and girdle to recreate the left pectoral skeleton. Since the pelvic skeleton of the whole-body *Neoceratodus* scan was not visible, we modeled the pelvic fin by scaling a copy of the pectoral fin skeleton to fit the position and dimensions of the pelvic flesh outline, and modeled the pelvic musculature by copying/scaling the pectoral muscle guides (see “[muscle guidelines](#)” below). We considered the latter a reasonable simplification because the overall dimensions of the pectoral versus pelvic musculature, in relation to the underlying skeleton, are broadly similar (see e.g.,^{28,29}). Furthermore, the

pectoral versus pelvic segments are sufficiently different in size (see [Figure 1A](#)) that any further difference caused by the exact placement of the respective musculature is likely quite minor in comparison.

Reference pose: Global coordinate system

Prior to constructing volumetric models, we arranged the skeleton of each specimen into a consistent reference pose in order to facilitate comparison across taxa ([Figure 1A](#)). First, we aligned each specimen into a consistent global coordinate system, with the x-axis pointing anteriorly, the y axis pointing to the left, and the z axis pointing dorsally ([Figure 1A](#)). The global origin was centered either between the acetabula (for tetrapods, following standard conventions⁶⁵) or at the base of the caudal fin (for fishes). This choice of global origin for each model ultimately reflects which anatomical 'landmark' provides the most comparable alignment of the overall body plan across our highly disparate sample. We aimed specifically to divide the overall body plan of each model into two functionally equivalent components: [1] the subset of the body where propulsion is principally generated (i.e., where the forward push on the body is occurring; $-x$ in our global coordinate system); versus [2] the subset of the body upon which this propulsion principally acts ($+x$ in our global coordinate system).

For fishes, we chose not to use the pelvis as the global-origin landmark given its tendency to be anteriorly displaced among actinopterygians (see e.g., Yamanoue et al.⁸⁶; see also *Amia* and especially *Periophthalmodon* in [Figure 1A](#)). This displacement means that such an alignment would not be functionally consistent with the inter-acetabular global origin of the tetrapod models, and thus would not constitute a comparable 'baseline' for downstream comparisons of overall trends in body plan (see next paragraph and "model evaluation" in [results](#)). Instead, we chose the base of the caudal fin as a more suitable landmark in actinopterygians, seeing as it is easily identifiable, positionally consistent (unlike the pelvis), and positionally comparable to the tetrapod pelvis (which itself occurs near the base of the tail). We also elected to use this 'tail-base' origin for *Neoceratodus* to maintain consistency with the protocol applied to the other fishes, recognizing that either landmark—tail-base or pelvis—would produce very similar results given the very close proximity of the pelvis to the caudal fin in this taxon (see [Figure 1A](#)).

Beyond serving to align our models, the position of the global origin is also important in evaluating trends in anteroposterior center-of-mass (COM_x) position across our sample, seeing as we normalized the raw COM_x coordinates for each model iteration as a percentage of the distance from the origin to the glenoid. To explore how our decisions regarding the global origin in fishes might impact our overall conclusions, we re-normalized the COM_x coordinates (see "analysis of mass properties" below) for the fish models using multiple different global-origin candidates ([Figure S4](#); [Table S5](#)): [A] the base of the caudal fin (as in the original analysis); [B] the posterior margin of the anal fin; [C] the anterior margin of the anal fin; and [D] the pelvis. For all comparisons, the tetrapod values were normalized against glenoacetabular distance (as in the original analysis). Finally, the results for *Neoceratodus* in [B] and [C] were normalized using glenoid–tailbase distance, given the fusion of the anal and caudal fins in this taxon.

Reference pose: Axial skeleton

We next straightened the axial skeleton of each model to be aligned horizontally along the global x-axis ([Figure 1A](#)). The two fossil models, *Ichthyostega* and *Eryops*, are exceptions to this generic reference pose: for *Ichthyostega*, the tail was left at a downward angle as in previous reconstructions³³; and, for *Eryops*, our skeletal model was based upon a photograph of a mounted specimen and so could not be adjusted as readily as our other models. Importantly, though, these exceptions do not affect the key parameters which form the focus of this study, namely body mass and the anteroposterior location of the whole-body center-of-mass (and the segment-wise contributions to both). Specifically, straightening the axial skeleton serves only to redistribute mass dorsoventrally, and so will not affect anteroposterior center-of-mass position or the mass of individual axial segments (the boundaries between which are dorsoventrally aligned). Regarding the flotation equilibrium simulations, the orientation of a given body segment will not affect the final equilibrium position reached by the overall model as long as that segment is entirely submerged (see also [Figure S5D](#)). This is the case for the tail of *Ichthyostega*, rendering it immaterial whether this segment is straightened out or directed downward. In contrast, our flotation simulations did show that the curved axial skeleton of *Eryops* partially protruded above the water line, which could affect the final equilibrium results; to accommodate for this, we therefore performed these simulations for *Eryops* using two sets of meshes: the original volumetric models for each variant (maximal mass, minimal mass, maximally anterior COM, maximally posterior COM), as well as a modified version in which each flesh and air-cavity mesh was dorsoventrally straightened to remove this curvature (see models in [Data S3](#)).

Reference pose: Appendicular skeleton

We aligned the appendicular skeleton into a reference pose balancing biological realism (i.e., actual joint articulation or geometry) versus standardisation (i.e., consistent and repeatable alignment across highly disparate anatomies). For the tetrapod models, this reference pose consists of a 'sprawling' posture ([Figure 1A](#)): the stylopod is held out laterally, with the distal articular surface horizontal; and the zeugopod and autopod are directed ventrally at 90° to the stylopod, with the palmar surface facing either posteriorly (forelimb) or medially (hindlimb). For the fish models, we aligned their fins along a single axis. For the lungfish, this pose matches that used for the tetrapod stylopod: the fins project laterally at 90° from the body, with the preaxial side of the fin pointing anteriorly ([Figure 1A](#)). For actinopterygians, we positioned the fins at an angle to the body, with the pectoral fins pointing posterolaterally at 45° to the main body axis and the pelvic fins pointing posteroventrally (45° lateral and 45° ventral to the main body axis) ([Figure 1A](#)). We chose this 'angled' posture for actinopterygians because, if positioned directly laterally as in the other specimens, the pectoral fin would intersect the skull and the pelvic fin would be almost completely disarticulated from the pelvic girdle. Although this pose introduces a posterior deflection of whole-body center-of-mass in actinopterygians relative to the other models (since the fins project

posterolaterally, rather than purely laterally), the fins contribute so little to overall whole-body mass (Figure 4A) and center-of-mass (Figure 4B) in actinopterygians that we did not consider this an issue in the present study.

Muscle guidelines

To more accurately delimit the boundaries of the proximal appendicular flesh volumes in sarcopterygians, we created several ‘guidelines’ to represent the likely paths of the superficial musculature, running as straight lines from inferred origins on the girdles to inferred insertions on the limbs (Figure S3). Rather than modeling all superficial muscles for each taxon, we specifically chose those positioned most anteriorly, posteriorly, dorsally, and ventrally, so as to delimit the likely maximal extent of the musculature. For mammals, we used the generalized muscle origins and insertions summarized by Böhmer et al.⁸⁷ For the crocodile, we used the digital muscle dissection of *Crocodylus porosus* provided by Klinkhamer et al.,⁸⁸ as well as information from Meers.⁸⁹ For *Ambystoma*, we used the muscle attachments reported by Walthall & Ashley-Ross⁹⁰ for the newt *Taricha*, with additional information from Molnar et al.^{28,29} For *Neoceratodus*, we placed the pectoral musculature based on Molnar et al.²⁸; given the lack of a visible pelvic skeleton in this microCT scan (see “specimen completeness” above), we then scaled and re-positioned these guidelines to approximate the pelvic musculature. Finally, for *Ichthyostega* and *Eryops*, where possible we used muscle attachment sites determined directly from fossils of these taxa (as reported by Molnar et al.^{28,29}); when such information was unavailable, we instead used the site(s) reconstructed for the closest major ancestral node (*Ichthyostega*: last common ancestor [LCA] of all tetrapods; *Eryops*: LCA of crown tetrapods; see Molnar et al.^{28,29}). In instances where these ancestral state reconstructions were ambiguous (i.e., when multiple origins and/or insertions were plausible), we placed guidelines for each possible combination of origin/insertion.

Model construction

Overall approach

We manually constructed volumetric models of each specimen using Rhinoceros 3D (Robert McNeel & Associates, v.7.SR36; RRID: SCR_014339), with the underlying skeleton acting as a guide for our reconstructions of soft-tissue geometries⁶² (Data S1). Building upon prior protocols, we reconstructed approximate flesh and air-space volumes using a hoop-based ‘spline’ method,^{61,62,65} in which octagonal hoops are fitted to the skeleton to define serial cross-sections of flesh and lighter-density air cavities (Figure S2; see Brassey⁶² and Bishop et al.⁴⁵ for comparisons of mass estimation approaches for extinct species).

To model the flesh, we first fitted symmetric ‘base’ hoops tightly to the underlying skeleton and, for appendicular segments, superficial muscle guides (Figures S2A and S3). The postcranial hoops were then systematically inflated and deflated to produce the maximum (larger, more square-shaped) and minimum (smaller, more diamond-shaped) plausible dimensions for each relevant body segment^{61,65,91} (Figure S2B). (The head was excluded from this expansion/deflation because flesh typically adheres quite closely to the skull, rendering the ‘base’ hoops a sufficient approximation for this segment.) This form of sensitivity analysis is important for capturing intraspecific variation, anatomical variation (e.g., some parts of the skeleton may provide less constraint on the girth of the overlying flesh), and inherent uncertainties associated with extinct taxa (in which soft-tissue anatomy may depart markedly from that observed in extant taxa). Because this method of creating segment variants broadly follows a ‘superellipse’ approach (see Allen et al.⁶¹ and Motani⁹² for further details), the dorsal and ventral halves of each octagonal hoop were therefore constructed as semi-ellipses.

To model the major internal air cavities, we fitted symmetric hoops within the head (for the buccal and nasal cavities), neck (for the trachea), and trunk (i.e., the visceral cavity, which was then modified to reflect the ‘lung’ anatomy appropriate for each taxon) (Figure S2A). The former three cavities were modeled following existing protocols,⁶⁵ whereas the lung reconstructions were based on the known respiratory anatomies of each extant group (see “lungs” below). As performed for the flesh volumes, we generated ‘maximum’ and ‘minimum’ plausible variants of the trachea and lungs for each taxon.

Finally, once the final geometries were generated for both the flesh segments and air cavities, we sealed these geometries to produce watertight volumes and exported them as 3D meshes.

Head

We modeled the head of each taxon by tightly fitting octagonal hoops to the underlying skeleton. Because flesh generally adheres closely to the contours of the head, this segment was treated as having a ‘constant’ geometry, obviating the ‘super-ellipse’ constraints described above. For some of our sample (namely, the fishes and extinct tetrapods), the head and pectoral girdle overlap anteroposteriorly, making the boundary between these segments less obvious to delineate. For these taxa, we defined the ‘head/trunk’ transition as occurring at the caudal limit of the head in actinopterygians (seeing as the pectoral girdle is quite minimal and almost entirely encapsulated within the head), and at the anterior limit of the pectoral girdle for the aforementioned sarcopterygian taxa (seeing as the pectoral girdle is larger and, although overlapped by the head, not totally encapsulated by it).

Buccal cavity

We modeled the buccal cavity by fitting octagons to the internal surface of the mandible and roof of the mouth. As for the head, the buccal cavity was treated as a ‘constant’ geometry, and so these hoops were constructed to be sagittally symmetrical but not necessarily semi-elliptical. In tetrapods, we defined the posterior extent of the buccal cavity as being level with the posterior extent of either the mandible or the cranium, whichever was more anterior in the taxon in question. For fishes, we set the posterior extent of the buccal cavity as level with the posterior extent of the overall head (regardless of the position of the mandible), to roughly encapsulate the presence of the ‘gill chambers’. In the actinopterygians, we modeled separate ‘dorsal’ and ‘ventral’ buccal cavity volumes, given the prominent pharyngeal skeleton in these taxa.

Nasal cavity

We modeled the nasal cavity by fitting octagonal hoops within the space between the orbits and nasal openings. We modeled this cavity for the lungfish and tetrapods, but not the actinopterygians; although the latter have an incurrent/excurrent passage between the external nares, this ‘nasal cavity’ is so small as to be negligible for our purposes. As for the head and buccal cavity, the nasal cavity was treated as a ‘constant’ geometry, and so these hoops were not constructed as semi-ellipses.

Trunk

For our purposes, we defined the trunk as extending: from the cranial limit of the pectoral girdle to the caudal limit of the pelvic girdle (tetrapods); from the cranial limit of the pectoral girdle to the cranial limit of the caudal fin (lungfish); or, from the caudal limit of the head to the cranial limit of the caudal fin (actinopterygians). For taxa without a distinct ‘neck’ (i.e., fishes, *Ichthyostega*, and *Eryops*), we re-used the posteriormost head hoop to serve as the anteriormost trunk hoop, in order to ensure a smooth transition between adjacent segments.

We constructed the trunk hoops as semi-elliptical in order to generate maximum and minimum variants of this segment. For the fishes, we placed semi-elliptical hoops along the entire trunk; for the tetrapods, we constructed semi-elliptical hoops until reaching the pelvis, at which point we again fitted the hoops in a non-elliptical (but still octagonal) manner as for the head. To model the dorsal and anal fins of fishes, we either encapsulated these median fins within the ‘trunk’ hoops (for the lungfish) or created ‘shrink-wrapped’ volumes of these fins using the mesh-editing software 3-matic (Materialise, v.17.0) and re-imported these constant volumes into Rhino (for the actinopterygians). We chose this latter approach for actinopterygians because these fins have so little flesh that hoops would inherently overestimate their dimensions. Because *Ambystoma* expresses only the dorsal component of the ribs, we approximated its trunk dimensions by fitting an ellipsoid between the pectoral and pelvic girdles, which we then used to guide the size of the base trunk hoops.

To create the ‘maximum’ variant of the trunk in extant tetrapods, we first uniformly inflated each base hoop’s vertices out from the hoop center by a factor of 1.2. For the base hoops located anterior to the pelvis, we then inflated the diagonal vertices by an additional factor of 1.207; this value corresponds to a superellipse that is midway between a circle and a square.⁹² The hoops fitted to the pelvis were excluded from this additional expansion because the cross-sections of these pelvic hoops were not constructed to be semi-elliptical.

To create the ‘maximum’ variant of the trunk in the other taxa (i.e., fishes, *Ichthyostega*, and *Eryops*), we took a modified approach, seeing as the trunk proceeds directly from the head in these taxa. First, we did not modify any base hoops that encircled both the head and the pectoral girdle, given that the dimensions of these hoops are tightly constrained by the head. For the trunk hoop closest to the glenoid, we inflated the diagonal vertices by a factor of 1.207. For the remaining trunk hoops (posterior to the glenoid), the approach differed by taxon: For *Ichthyostega* and *Eryops*, we first inflated each remaining hoop uniformly by a factor of 1.2, then inflated the diagonal vertices by an additional factor of 1.207 for the base hoops located anterior to the pelvis. For the fishes, we followed the same approach, except that the second step (scaling of the diagonal vertices) was applied along the entire trunk; this latter step is appropriate since the pelvis is quite small, meaning that we could fit semi-elliptical hoops along the entire trunk. Because the dorsal and anal fins provide an additional, tight constraint on the dorsoventral extent of the trunk flesh in actinopterygians, we performed a final step after inflating the trunk hoops: for any trunk hoops occurring along the dorsal fin(s), we manually translated the dorsalmost vertex of the inflated hoop ventrally, so that it was ultimately positioned just dorsal to the neighboring diagonal vertices; and, for any trunk hoops occurring along the anal fin, we manually translated the ventralmost vertex of the inflated hoop dorsally, so that it was ultimately positioned just ventral to the neighboring diagonal vertices.

For all taxa, the ‘minimum’ variant of the trunk simply constituted the base hoops as originally constructed, seeing as these had already been fitted tightly to the underlying skeleton.

As a final step for the actinopterygian models, we ‘fused’ each trunk variant with the ‘shrink-wrapped’ fin-ray volumes described above (using Boolean operations in either Rhino or 3-matic), thus creating the final trunk volumes.

Lungs

We did not construct ‘lung’ volumes for *Periophthalmodon*, given its lack of a swimbladder (e.g., Gonzales et al.⁹³). For the remaining taxa, we modeled the lungs by first using hoops to create an overall ‘visceral cavity’ volume, which we then cropped to create plausible maximum and minimum lung geometries for each taxon (see below). We placed the anteriormost visceral hoop at the anterior extent of the chest, and the posteriormost visceral hoop at either the anterior extent of the pelvis (in non-mammalian tetrapods), the posterior extent of the ribcage (in mammals, corresponding to the level of the diaphragm), or the anterior extent of the anal fin (in fishes). We then placed additional hoops between these endpoints as needed to capture the internal contours of the trunk. To more closely follow the internal surfaces of the ribs, vertebrae, and gastralia, we used ~10–12 vertices per hoop, rather than an octagon. As noted above for the trunk, since *Ambystoma* only expresses the dorsal component of the ribs, we therefore used the aforementioned ‘trunk proxy’ ellipsoid to guide the dimensions of the visceral hoops, fitting them closely to the ventrolateral margins of this ellipsoid.

Upon completing this base ‘visceral cavity’ volume, we then modified it to create either ‘mammalian’, ‘reptilian’, ‘salamander-style’, or ‘swimbladder-style’ lungs, each of which had a maximum and minimum variant. We devised these ‘styles’ using a combination of existing volumetric modeling protocols,^{61,65} literature sources,^{94,95} and personal observations or knowledge of vertebrate anatomy. To construct ‘mammalian’ lungs, we used the original ‘visceral cavity’ volume as the ‘maximum’ lung variant (seeing as this was already constructed in the mammal models to fill just the ribcage), and cropped this volume to the anteriormost 33% of its

original length to create the ‘minimum’ variant. We applied this technique to the three mammals in our study. To construct ‘reptilian’ lungs, we cropped the overall ‘visceral cavity’ to either the anteriormost 50% or anteriormost 25% of its original length, comprising the ‘maximum’ and ‘minimum’ lung variants, respectively. We applied this technique to the crocodile, as well as *Ambystoma*, *Eryops*, and *Ichthyostega* as a conservative approach to these latter taxa. To construct ‘salamander-style’ lungs, we first cropped the overall ‘visceral cavity’ volume to the dorsalmost 50% of its original height and divided it in half to create left and right ‘lobes’. To create the ‘maximum’ lung variant, we cropped each lobe to the lateralmost 75% of its original width. To create the ‘minimum’ lung variant, we cropped each lobe to the middle 25% of its original width and anteriormost 50% of its original length. We applied this technique to *Ambystoma*, *Eryops*, and *Ichthyostega*. To construct ‘swimbladder-style’ lungs, we first cropped the overall ‘visceral cavity’ volume to the dorsalmost 50% of its original height. We then cropped it to either the middle 50% or middle 25% of its original width, comprising the ‘maximum’ and ‘minimum’ lung variants, respectively. We applied this technique to *Amia* and *Neoceratodus*.

Trachea

We modeled a trachea for all tetrapods in our sample, as well as for the fishes in which the buccal cavity is connected via a duct to the swimbladder/lungs (i.e., *Amia* and *Neoceratodus*). To model the trachea, we placed circular octagonal hoops along the neck, just ventral to the cervical centra, with the anteriormost tracheal hoop aligned with the posterior buccal hoop and the posteriormost tracheal hoop aligned with the anteriormost visceral hoop. We set the diameter of these octagons as equal to the height of the posteriormost buccal hoop for that taxon, and constructed each hoop at the same angle as the accompanying cervical vertebra. To create the ‘maximum’ variant of the trachea, we inflated each base hoop uniformly by a factor of 1.2. To create the ‘minimum’ variant, we deflated each base hoop uniformly by a factor of 0.8.

Neck

We modeled the neck as connecting the posteriormost head hoop to the anteriormost trunk hoop. We created additional semi-elliptical hoops between these endpoints as needed, using the dimensions of the tracheal hoops and the cervical vertebrae to inform the size of the base ‘neck’ geometry. To create the ‘maximum’ variant of the neck, we first inflated each base hoop uniformly by a factor of 1.2, then inflated the diagonal vertices by an additional factor of 1.207. The anteriormost neck hoop was excluded from this adjustment, since the dimensions of this hoop are tightly constrained by the head. To create the ‘minimum’ variant of the neck, we deflated the diagonal vertices by a factor of 0.853; this value corresponds to a superellipse that is midway between a diamond and a circle.⁹² The anteriormost and posteriormost neck hoops were excluded from this adjustment, since the minimum dimensions of these hoops are already tightly constrained by the head and trunk, respectively.

Tail

To ensure continuity between adjacent segments, we re-used the posteriormost trunk hoop to serve as the anteriormost tail hoop. As mentioned above for the trunk, this hoop was placed at the caudal limit of the pelvic girdle in tetrapods and at the cranial limit of the caudal fin in fishes. We then modeled the remainder of the tail by tightly fitting semi-elliptical, octagonal hoops to the underlying skeleton. In sarcopterygians (including tetrapods), we placed these hoops along the full length of the tail. In actinopterygians, we placed the final tail hoop at the base of the caudal fin rays; seeing as actinopterygian fin rays have very little flesh, we did not model this distal part of the fin using hoops, but instead ‘shrink-wrapped’ this sub-segment of the skeleton in 3-matic to create a tightly-fitted ‘fin-ray’ mesh which we then re-imported into Rhino (see also “trunk” above).

For the tetrapods in our sample, we also created a second set of tail hoops by expanding the aforementioned ‘base’ hoops by a pre-established set of ‘inflation factors’; these factors were derived by Allen et al.⁶¹ based on saurian tails, and provide a close approximation of the relationship between skeletal versus flesh dimensions in this group. Although these ‘inflation factors’ have only been validated in saurians, we applied this technique to all of the tetrapods in our sample as it provides a standardized and anatomically-plausible approach to capturing the general ‘fleshiness’ of tetrapod tails. In order to model the plausible dimensions of the tetrapod tails as thoroughly as possible, we created maximum and minimum variants (see below) using both the base and ‘saurian-inflated’ hoops.

To create the ‘maximum’ variant of the tail, we first inflated each base hoop uniformly by a factor of 1.2. For the fish models, we then further inflated the diagonal vertices of all hoops by a factor of 1.207. For the tetrapod models, we applied this additional expansion to all hoops except the anterior-most one, in order for the ‘maximum tail volume’ to be continuous with the ‘maximum trunk volume’. Finally, for the actinopterygians, we translated the dorsalmost and ventralmost vertices of the expanded hoops as described above for the trunk. To create the ‘minimum’ variant of the tail, our approach differed depending on whether the ‘saurian inflation factors’ had been applied or not to the hoops in question. For the original (non-‘saurian-inflated’) base hoops, these hoops were already fitted tightly to the underlying skeleton and so already constituted a minimum-volume variant. For the ‘saurian-inflated’ version of the base hoops, we deflated the diagonal vertices of each hoop by a factor of 0.853, except for the proximal-most hoop (which had been closely fitted to the pelvis and thus was left unaltered). As a final step for the actinopterygian models, we ‘fused’ each tail variant with the ‘shrink-wrapped’ caudal fin-ray volumes described above, thus creating the final tail volumes.

Pelvic girdle and thigh

Given the irregular shape of the pelvic girdle, we manually outlined its outer margin using a series of connected line segments, with the specific number of lines differing for each taxon as needed to closely encapsulate both the pelvis and key superficial musculature of the proximal hindlimb (see “muscle guidelines” above). We then delimited the distal extent of the thigh using an elliptical hoop placed at the knee, tilted at 45° to accommodate the flexed knee posture and again closely fitted to the underlying skeleton and muscle

guides. We also placed at least one additional elliptical hoop along the thigh, in order to ensure that the overall geometry of this segment closely followed the underlying musculoskeletal anatomy.

Crus

We delimited the proximal extent of the crus using the distalmost ‘thigh’ hoop, and the distal extent of the crus using an elliptical hoop fitted tightly to the bones at the proximal end of the ankle. We then created a final crus hoop one-third of the distance between these proximal and distal octagons. To ensure the proper spacing, we first constructed line segments to connect the corresponding vertices on the proximal versus distal hoops, then divided each line into three equal sections and manually constructed an octagon connecting the proximal one-third of each line. To represent the distal limb musculature, we then translated this hoop laterally (in relation to the overall model; cranially in the frame of the crus) along one-quarter of its length, then expanded the anterior (medial, in the frame of the crus) three and posterior (lateral) three vertices of this final hoop by 25%.

Ankle/proximal pes

We modeled the proximal extent of this segment using the distalmost ‘crus’ hoop, and its distal extent using an elliptical hoop fitted tightly to the base of the digits. We then placed a third elliptical hoop midway along the segment, adding additional hoops as needed to closely fit the underlying skeletal anatomy.

Pedal digits

Rather than modeling each digit separately, we instead created a single, mitten-like volume to encapsulate all of the phalanges. The distalmost ‘ankle’ hoop was used as the proximalmost ‘toe’ hoop, with additional elliptical hoops placed along the foot, terminating just distal to the longest digit.

Pectoral girdle

As for the pelvic girdle, we manually outlined the outer margin of the pectoral girdle using a series of connected line segments, which we fitted closely to the underlying skeleton and muscle paths (see “[muscle guidelines](#)” above). To delimit the distal extent of the pectoral girdle, we fitted an elliptical hoop at the proximal end of the deltopectoral crest, with dimensions just large enough to encompass the muscle guides, deltopectoral crest, and any other protrusions from the proximal humerus or lateral face of the girdle.

Humerus

The distal ‘pectoral’ hoop also served as the proximalmost ‘humerus’ hoop. We delimited the distal extent of the upper arm using an elliptical hoop placed at the elbow, tilted at 45° to accommodate the flexed elbow posture and again closely fitted to the underlying skeleton and muscle guides. We then placed additional elliptical hoops along the humerus, if needed, to ensure that the overall geometry of this segment closely followed the underlying musculoskeletal anatomy.

Forearm

We modeled the forearm similarly to the crus (see “[crus](#)” above): the distalmost ‘humerus’ hoop was used as the proximalmost ‘forearm’ hoop, the distal forearm was modeled using an elliptical hoop fitted tightly to the bones at the proximal end of the wrist, and a final hoop was placed one-third of the distance between these termini. We drew this final hoop using the same steps as outlined above (see “[crus](#)”) for the corresponding ‘crus’ hoop (i.e., using polylines divided into three equal segments); however, unlike the crus, we did not translate or scale this hoop by any set amount, instead simply expanding it laterally from its medial-most vertex until it encompassed the underlying skeleton as tightly as possible.

Wrist/proximal manus

We modeled the wrist in the same manner as the ankle (see “[ankle/proximal pes](#)” above): first, we modeled the proximal extent of this segment using the distalmost ‘forearm’ hoop; then, we modeled its distal extent using an elliptical hoop fitted tightly to the base of the digits; and finally, we placed a third elliptical hoop midway along the segment, adding additional hoops as needed to closely fit the underlying skeletal anatomy.

Manual digits

We modeled the fingers in the same manner as the toes (see “[pedal digits](#)” above), creating a single volume to encapsulate all of the phalanges. We used the distalmost ‘wrist’ hoop as the proximalmost ‘finger’ hoop and placed additional elliptical hoops along the hand, terminating just distal to the longest digit.

Paired fins

To model the appendicular segments of actinopterygians, we started by manually outlining the borders of the pelvic and pectoral girdles as described above for tetrapods (see “[pelvic girdle and thigh](#)” and “[pectoral girdle](#)”). As an exception, the pelvic girdle of *Amia* was simple enough in anatomy that we simply fitted octagonal hoops along its length; these ‘pelvic’ hoops were not modified into minimum or maximum variants, and so were not constructed as semi-ellipses. For the fins themselves, we used a different approach for actinopterygians versus the lungfish. For *Neoceratodus*, we placed elliptical hoops along the full length of the fins, fitted tightly to the underlying fin skeleton and muscle paths. For the actinopterygians, we followed a similar approach as for their caudal fin (see “[tail](#)” above): First, we constructed hoops only along the base of the fin (as this is its only ‘fleshy’ component), placing one elliptical hoop where the radials meet the fin rays and, if needed, a few additional elliptical hoops between this junction and the girdle outline to closely follow the underlying skeleton. We then modeled the fin rays by ‘shrink-wrapping’ this part of the fin (using the ‘Wrap’ function in 3-matic) and re-importing the resulting meshes into Rhino.

Maximum and minimum appendicular variants

To create the ‘maximum’ variants of the appendicular segments, we first inflated each base hoop uniformly by a factor of 1.2, then inflated the diagonal vertices by an additional factor of 1.207. We did not modify the pelvic or pectoral girdle outlines, as these are

closely constrained by the underlying musculoskeletal anatomy. To create the ‘minimum’ variants of the appendicular segments, our approach differed by taxon. For the lungfish, we used the base hoops as the minimum volume, since these had already been fitted tightly to the underlying skeleton and muscle guidelines. For the actinopterygians, we deflated the diagonal vertices of all hoops by a factor of 0.853. For the tetrapods, we used the base hoops for the humerus and thigh (including the hoops located at the elbow and knee), since these had already been fitted tightly to the underlying skeleton and muscle paths; for the remaining hoops, we deflated the diagonal vertices by a factor of 0.853. For all taxa, we left the pelvic and pectoral girdle outlines unmodified, as these geometries had already been closely fitted to the underlying musculoskeletal anatomy. As a final step for the actinopterygian models, we ‘fused’ each paired fin variant with the ‘shrink-wrapped’ fin-ray volumes described above (using Boolean operations in either Rhino or 3-matic), thus creating the final fin volumes.

Model finalization

Removal of segment overlap

Once the final variant volumes were constructed, we used Boolean subtraction in Rhino to minimize overlap between the axial and proximal appendicular segments (Figure S6). Given the ‘population-based’ approach used herein to calculate mass properties, it is impossible to perfectly eliminate potential overlap for each segment in each model, seeing as these overall models are randomly generated. Instead, we addressed this limb/body overlap by creating ‘maximum’ and ‘minimum’ cropped versions of each affected appendicular segment (i.e., thigh, shoulder, and sometimes humerus for tetrapods; fins for fishes) (Figures S6B and S6C). While some amount of segment overlap is ultimately inevitable with this approach, it is minimized as much as possible; furthermore, we consider any potential error caused by this overlap as being greatly outweighed by the new advantages introduced by our ‘population-based’ approach.

The ‘maxCropped’ version reflects the maximum possible dimensions of the appendicular segment when cropped; i.e., the ‘maximum’ variant of the appendicular segment-in-question, and the ‘minimum’ variant(s) of the cutting object(s) (Figure S6B). For example, the ‘maxCropped’ shoulder for *Ambystoma* would comprise the ‘maximum shoulder’ variant constructed above, cropped using the ‘minimum neck’ and ‘minimum trunk’ variants. Conversely, the ‘minCropped’ version reflects the minimum possible dimensions of the appendicular segment when cropped; i.e., the ‘minimum’ variant of the appendicular segment-in-question, and the ‘maximum’ variant(s) of the cutting object(s) (Figure S6C). For example, the ‘minCropped’ shoulder for *Ambystoma* would comprise the ‘minimum shoulder’ variant constructed above, cropped using the ‘maximum neck’ and ‘maximum trunk’ variants.

Export of final volumes

Once the final segment variants had been created, we exported each volume from Rhino as an STL-format mesh, then converted these meshes to OBJ format in 3-matic for compatibility with MATLAB. All meshes are available in the Supplemental Data accompanying this publication.

Further sensitivity analysis of *Ichthyostega*

In addition to uncertainties in soft-tissue reconstruction, the results for extinct species may also be subject to error due to inaccuracies in the underlying skeletal reconstruction. This is particularly pertinent for the *Ichthyostega* model, which is a composite of multiple specimens from multiple species³³ and which differs from previously published 2D reconstructions,^{7,17,54} most notably in the relative size of the pelvis and hindlimb (which are appreciably smaller than the forelimb and pectoral girdle in the reconstruction of Pierce et al.³³). To explore the consequences of this reconstruction, we produced additional variants of the hindlimb and pelvis of *Ichthyostega* by ‘inflating’ the original model to varying degrees (Figure S1). First, we created an ‘equal-hindlimb’ variant by increasing the flesh volume of the pelvic girdle and hindlimb to match that reconstructed for the ‘minimum’ pectoral girdle and forelimb variant. Second, we created a ‘greater-hindlimb’ variant based on the body proportions of our extant tetrapod sample, in which the hindlimbs are notably larger than the forelimbs. Specifically, among our extant tetrapod models, *Ambystoma* exhibited the lowest ratio of pelvic:pectoral volume (1.27), whereas *Crocodylus* exhibited the greatest ratio (1.61). Therefore, to create our ‘greater-hindlimb’ variant for *Ichthyostega*, we increased the volume of the pelvic girdle and limb such that it was 1.61× the volume of the ‘maximum’ pectoral girdle and limb variant.

To test how these different reconstructions would affect the resultant mass properties of *Ichthyostega*, we performed each analysis herein using three ‘versions’ of this taxon: a ‘best-estimate’, an ‘inflated’ version, and an ‘overall’ version (Figure S1). The ‘best-estimate’ model uses the original (non-inflated) hindlimb volumes, reflecting the premise that Pierce et al.³³ had indeed accurately scaled the various specimens of *Ichthyostega* when creating their 3D skeletal composite; this version is referred to herein as simply ‘*Ichthyostega*’. The ‘inflated’ model uses the ‘equal-hindlimb’ and ‘greater-hindlimb’ variants as its minimum and maximum hindlimb, respectively, reflecting a scenario in which the reconstruction by Pierce et al.³³ underestimated the hindlimb dimensions of *Ichthyostega*. The ‘overall’ model uses the original minimum-hindlimb and inflated ‘greater-hindlimb’ variants as its respective minimum and maximum hindlimb, thus representing the full range of hindlimb dimensions reconstructed herein.

QUANTIFICATION AND STATISTICAL ANALYSIS

Analysis of mass properties

Mass property estimation

We calculated mass and center-of-mass (COM) location via custom scripts in MATLAB (MathWorks, USA, v.R2023b; RRID: SCR_001622; Code S1), which used the mass properties of each individual body segment (Data S2) to compute whole-animal and segment-wise mass and COM (Tables S2; S3; Data S4). The whole-body COM calculation followed the equation

$$\mathbf{p}_{\text{COM}} = \left(\frac{\sum_{i=1}^n m_i x_i}{\sum_{i=1}^n m_i}, \frac{\sum_{i=1}^n m_i y_i}{\sum_{i=1}^n m_i}, \frac{\sum_{i=1}^n m_i z_i}{\sum_{i=1}^n m_i} \right), \quad (\text{Equation 1})$$

where m_i denotes the mass of the i th body segment and (x_i, y_i, z_i) denotes the COM of the i th body segment in the global coordinate system. In the present study, +x denotes the anterior direction, +y the left side, and +z the global ‘up’ direction (Figure 1A). Each term in the numerator of Equation 1 defines the i th segment’s first mass moment (FMM), which describes its contribution to overall COM in each direction. Thus, in addition to providing estimates of whole-animal mass and COM location, it is also possible to assess the differential contribution of each body segment to whole-body mass properties in a given animal.⁶⁵ The density of flesh volumes was nominally set at 1,000 kg/m³, whereas that of the lungs and other air spaces (e.g., buccal cavity, trachea) was set at 0 kg/m³ (cf.^{96,97}). We also repeated our analyses with the flesh density set to 850 kg/m³ (see Tables S2; S3; Data S4).

Assessment of intraspecific variation

Recognizing that most individuals of a species will likely fall somewhere between the upper and lower possible bounds of variation, previous studies have typically taken the midpoint between the ‘maximum’ and ‘minimum’ variants of each segment as a proxy for the ‘average’ individual of a given taxon (see e.g.,^{45,65,84}). However, this approach not only reduces potential intraspecific variation down to a single number, but also implicitly assumes that this variation is symmetrically distributed between upper and lower bounds, such that a single midpoint value can sufficiently summarize this variation. To provide a more nuanced perspective on reconstruction error and intraspecific variability, we instead used Monte Carlo resampling to mimic potential variation throughout a hypothetical population (Figure 1C; Code S1). Rather than relying on a single ‘average’ (or ‘maximum’, or ‘minimum’) body-mass model for a given taxon, we instead randomly generated the mass properties for each body segment using a distribution bounded by the ‘maximal’ and ‘minimal’ variants of that segment, thus mimicking ‘randomly sampling’ an individual from that taxon. Repeated resampling in turn produces a distribution of plausible values in the mass properties for a given species, which can ultimately be compared to the distributions generated for other species. We performed this sampling for a total of 10,000 replicates, nominally drawing from a normal distribution (scaled such that maxima and minima equated to 3 σ); we also repeated our assessments using a uniform distribution, which offered a qualitatively similar but quantitatively more conservative assessment (see Tables S2 and S3; Data S4).

Analysis of flotation equilibrium

Buoyancy simulations

In addition to reconstructing the mass properties of each taxon, we also examined the influence of these properties in an aquatic context. We accomplished this by calculating the state of flotation equilibrium in the sagittal plane, following the general approach of previous studies by Henderson.^{52,53} To do so, we used custom MATLAB scripts (Code S2) to run a pseudo-dynamic, rigid-body simulation of the whole-animal model (Data S3) immersed in water, setting the waterline at $z = 0$ (Figure 1D). In each iteration of the simulation, the weight force due to gravity (\mathbf{F}_W) and the buoyant force due to immersion (\mathbf{F}_B) were computed for the current configuration of the model. Whereas \mathbf{F}_W acts downward through the COM of the body, \mathbf{F}_B acts upward through the center-of-buoyancy (COB), equal to the COM of the volume of water displaced by just the submerged part of the model. Imbalance in the magnitude of downward and upward forces resulted in an adjustment of vertical position in the succeeding iteration, while a non-zero moment of \mathbf{F}_B about the COM of the body resulted in an adjustment of model orientation (in the sagittal plane) in the succeeding iteration. Flotation equilibrium is achieved when there is balance between \mathbf{F}_W and \mathbf{F}_B (i.e., Archimedes’ Principle):

$$\mathbf{F}_W + \mathbf{F}_B = \mathbf{0}, \quad (\text{Equation 2})$$

$$Mg + V_{\text{submerged}} \rho_{\text{water}} g = 0, \quad (\text{Equation 3})$$

and the COB and COM are vertically aligned, such that moment of \mathbf{F}_B about the COM is zero:

$$\mathbf{F}_B \times (\mathbf{p}_{\text{COB}} - \mathbf{p}_{\text{COM}}) = \mathbf{0}, \quad (\text{Equation 4})$$

where M is whole-animal mass, g is the acceleration due to gravity (9.80665 m/s²), $V_{\text{submerged}}$ is the volume of the model currently submerged, and ρ_{water} is the density of fresh water (1,000 kg/m³). A simulation was terminated when force and moment imbalance fell below a pre-set threshold (i.e., minimal further adjustments would occur), indicating that equilibrium had been reached; all simulations converged within 2 min using a standard 2.8 GHz Intel Core i7 processor, and frequently much faster. The simulation thereby produced an ‘equilibrium pose’ representing how the whole-body model was oriented in the sagittal plane.

For each taxon, we performed flotation simulations with four model variants (maximal mass, minimal mass, maximally anterior COM, maximally posterior COM) and two bulk densities assigned to flesh segments (1,000 and 850 kg/m³). To generate these model variants, we used custom MATLAB code to calculate the whole-body mass and COM of all possible combinations of all segment variants (Code S3; Data S2), which allowed us to determine the combinations of segment meshes that produced the aforementioned ‘extremes’ of each taxon’s overall body plan (Data S3). Once each simulation had terminated, we recorded the pitch angle by calculating the difference in the model’s sagittal plane orientation in the equilibrium pose compared to the neutral posture (Figure 1D; Table S4).

Data processing and visualization

All summary values (as reported in the [results](#)), tables, and plots were generated using R⁹⁸ (v.4.3.2; RRID: SCR_001905) and RStudio⁹⁹ (v.2023.12.1.402; RRID: SCR_000432) (Code S4).